

## Non-local effects on the non-linear modes of vibration of carbon nanotubes under electrostatic actuation

Pedro Ribeiro

DEMec/INEGI, Faculdade de Engenharia, Universidade do Porto, R. Dr. Roberto Frias, s/n, 4200-465 Porto, Portugal



### ARTICLE INFO

*Article history:*

Received 8 December 2015

Received in revised form

22 May 2016

Accepted 21 July 2016

Available online 24 August 2016

*Keywords:*

Carbon nanotubes

Electrostatic

Non-local

Non-linear modes of vibration.

### ABSTRACT

Carbon nanotubes (CNTs) based NEMS with electrostatic sensing/actuation may be employed as sensors, in situations where it is fundamental to understand their dynamic behaviour. Due to displacements that are large in comparison with the thickness and to the non-linearity of the electrostatic force, these CNT based NEMS operate in the non-linear regime. The knowledge of the modes of vibration of a CNT provides a picture of what one may expect from its dynamic behaviour not only in free, but also in forced vibrations. In this paper, the non-linear modes of vibration of CNTs actuated by electrostatic forces are investigated. For that purpose, a *p*-version finite element type formulation is implemented, leading to ordinary differential equations of motion in the time domain. The formulation takes into account non-local effects, which influence the inertia and the stiffness of CNTs, as well as the electrostatic actuation. The ordinary differential equations of motion are transformed into algebraic equations of motion via the harmonic balance method (HBM) and then solved by an arc-length continuation method. Several harmonics are considered in the HBM. The importance of non-local effects, combined with the geometrical non-linearity and with the action of the electrostatic force, is analysed. It is found that different combinations of these effects can result in alterations of the natural frequencies, variations in the degrees of softening or hardening, changes in the frequency content of the free vibrations, and alterations in the mode shapes of vibration. It is furthermore found that the small scale, here represented by the non-local theory, has an effect on interactions between the first and higher order modes which are induced by the geometrical and material non-linearities of the system.

© 2016 Elsevier Ltd. All rights reserved.

### 1. Introduction

With advances in nanotechnology, it is becoming possible to use nanostructures, like the Carbon Nanotubes (CNTs) of interest in this paper, in a number of important applications, including: the detection of particular molecules or cells, which may be related to specific diseases; mass sensing; force sensing; nanoswitches; and nanoactuators [1–7]. The resonance frequency and other dynamic characteristics are of chief importance in these nanoscale devices, playing a critical role on detection sensitivity. Clearly, an accurate estimation of their natural frequencies is fundamental in order to use CNTs as resonant sensors [7,8]. Regarding the vibratory properties, it is important to take into account that CNTs may experience displacements with amplitudes of the order of their very small diameter, causing a type of nonlinearity known as geometric nonlinearity [8–13]. In this case, the tensile forces on a CNT change, altering the restoring forces and the displacement amplitudes, in a fashion that cannot be predicted by linear models.

Moreover, as a consequence of the geometrical non-linearity, the resonance frequency and the mode shapes of vibration change with the vibration amplitude. Geometrical nonlinearity may also lead to modal coupling [14–17].

Advantages attributed to electrostatic actuation include leading to simple and relatively easy to fabricate structures, requiring low power consumption, having high efficiency and quick response; therefore, this is a popular actuation mechanism in micro and nanoelectromechanical systems (NEMS) [2,18]. In electrostatic actuation there is one fixed and one movable electrode (in our case, the Carbon Nanotube) and a voltage difference is applied between the two. The electrostatic force is a highly non-linear function of the distance between the electrodes involved [19–21], further enriching the dynamic behaviour of NEMS. For example, whilst a straight beam vibrating with large amplitudes typically experiences hardening, in the presence of electrostatic forces softening may appear [8,11,19,22–24]. Non-linearity in electrostatically actuated CNTs has motivated some studies in statics and dynamics. One example is provided by Dequesnes et al. [25], where pull-in is studied in several Carbon Nanotubes. For that

E-mail address: [pmleal@fe.up.pt](mailto:pmleal@fe.up.pt)

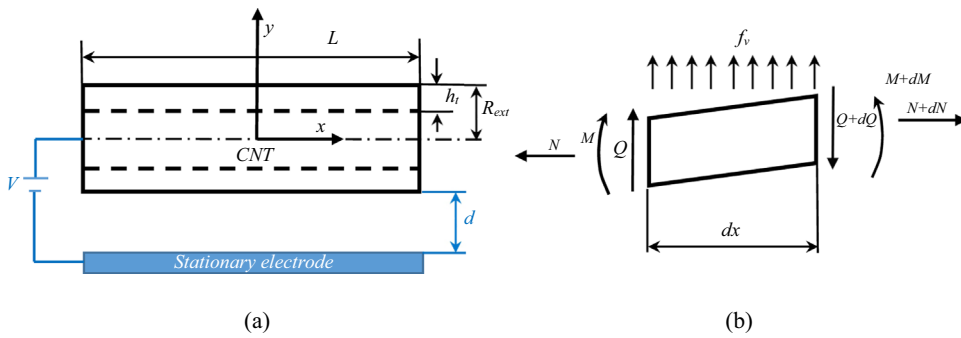


**Fig. 1.** Representation of: (a) CNT, electrode and Cartesian coordinate system; (b) free body diagram of an infinitesimal element.

purpose, the authors derived an expression for the electrostatic force exerted on the CNT, considering that this is the force exerted by a plane on a cylinder. Ke et al. [26] obtained an equivalent expression for the electrostatic force and confirmed that geometrical non-linearity can have a substantial effect on the pull-in voltage of CNTs. In [8], an investigation of non-linear vibrations of CNTs when actuated by a DC load and an AC load is carried out. It is shown that geometrical non-linearity has an important influence on the vibrations of doubly-clamped CNTs. In [27], a non-local elasticity theory is employed to investigate the deflections (in static problems) and pull-in. It is concluded that non-local effects lead to higher pull-in voltages. Rasekh and Khadem [28] analyse the vibrations of a CNT cantilever, considering non-linear effects due to large displacements, electrostatic forces and inertial terms. Galerkin's method and direct, time domain, numerical integration are used. It is found that non-linear effects can be very important in the problem studied.

CNTs are very small structural elements, where the elasticity theory that is valid at macro scales can fail [29,30]. The nonlocal elasticity theory of Eringen [31,32] has been proposed as a way to obtain theoretical models that are valid at small scales. In this theory, the stress field at a reference point in an elastic continuum depends not only on the strain at that point but also on strains at all other points in the domain. Non-local elasticity provides an alternative to atomistic simulations [7,33,34], which demand too much computational effort, and to formulations based on classical continuum mechanics, which can fail in nanostructures, because they do not take scale effects into account [1,35,36]. In the case of beams, the integral-partial differential equations of Eringen's non-local elasticity can be reduced to partial differential equations [32]. Studies indicate that small size effects in beams can be captured by a non-local elasticity theory and that, therefore, it can be applied to derive mathematical models for nanosized beams [34,37,38]. Related with this aspect and also of interest to the present work are references [39,40], where it was demonstrated that the non-local elasticity affects the modes of vibration of CNTs in the geometrically non-linear regime. In the two former references, it was assumed that the oscillations in the non-linear regime are harmonic.

In non-linear, as in linear, problems, the natural modes of vibration provide information that is fundamental to understand the dynamic behaviour of a structure. In the present work, it is intended to investigate the non-linear modes of vibration of CNTs under DC electrostatic actuations. For that purpose, a continuum mechanics based  $p$ -version finite element [15,16], which takes into account the geometrical and electrostatic non-linear effects, is presented. In order to achieve models that are valid at nanoscales, the  $p$ -element employs the nonlocal elasticity theory of Eringen [26,27,41]. Furthermore, the non-local effects of the electrostatic force are taken into account. The  $p$ -version FE equations of motion are ordinary differential equations in the time domain; they are

converted to the frequency domain by the harmonic balance method (HBM). The ensuing frequency domain equations are solved by an arc-length continuation method [14,15]. By considering several harmonics, it is demonstrated that higher harmonics can be fundamental in the oscillations of the CNTs. The influence of non-local effects, in combination with electrostatic forces, on the non-linear modes of vibration of CNTs is discussed.

## 2. Modelling and analysis approach

### 2.1. Partial differential equations of motion

In [32], Eringen presented non-local constitutive relations as second-order differential equations, which in the case of Bernoulli-Euler beams reduce to just one differential constitutive equation [41]

$$\sigma_x(x, t) - \mu \frac{\partial^2 \sigma_x(x, t)}{\partial x^2} = E \varepsilon_x(x, t) \quad (1)$$

In the former equation,  $\sigma_x(x, t)$  represents the axial stress,  $\varepsilon_x(x, t)$  the axial strain,  $E$  the Young modulus and  $\mu$  a non-local parameter. The latter is  $\mu = (e_0 a)^2$ , where  $a$  is an internal characteristic length (as the lattice parameter, granular distance, distance between C-C bonds) and  $e_0$  is a constant that depends on the material [32,36]. These parameters can be obtained via experiments, molecular mechanics or molecular dynamics.

Following Bernoulli-Euler's beam theory, the longitudinal displacement,  $\bar{u}(x, y, t)$ , and the transverse displacement (in direction  $y$  of Fig. 1),  $\bar{v}(x, y, t)$ , of any point of a beam are given by

$$\begin{cases} \bar{u}(x, y, t) = u(x, t) - y \frac{\partial v}{\partial x}(x, t), \\ \bar{v}(x, y, t) = v(x, t), \end{cases} \quad (2)$$

where  $u(x, t)$  and  $v(x, t)$  represent displacements of points on axis  $x$ , which is here the axis that contains the geometric centres of the cross sections, and  $t$  represents time. In Fig. 1(a) one can see a depiction of a beam with hollow circular cross section, representing a Carbon Nanotube. The length of the CNT is  $L$ , the external radius is represented by  $R_{ext}$  and  $h_t$  indicates the effective tube thickness; the internal radius, which is not represented in the figure, is  $R_{int}$ ; letter  $d$  represents the distance between the electrode and the CNT in the undeformed state, also known as initial gap width or undeformed gap space. Because it is important to justify the signs in some of the equations that follow, signs which differ from the ones that can be found in some literature, the free body diagram of an infinitesimal CNT element is represented in Fig. 1(b).  $Q(x, t)$  – function arguments not written in the figure – is the transverse force (a stress resultant), the meaning of other symbols is given afterwards. External longitudinal forces are not

represented, in order to simplify the figure and because this type of force does not appear in the problem under consideration in this paper.

Considering displacements that can be moderately large, a Von Kármán type strain displacement relation is assumed

$$\epsilon_x(x, y, t) = \frac{\partial u(x, t)}{\partial x} + \frac{1}{2} \left( \frac{\partial v(x, t)}{\partial x} \right)^2 - y \frac{\partial^2 v(x, t)}{\partial x^2}. \quad (3)$$

From Eqs. (1) and (3), result the following relations for the longitudinal force,  $N(x, t)$ , and for the bending moment,  $M(x, t)$  [40,42]:

$$N(x, t) - \mu \frac{\partial^2 N(x, t)}{\partial x^2} = EA \left( \frac{\partial u(x, t)}{\partial x} + \frac{1}{2} \left( \frac{\partial v(x, t)}{\partial x} \right)^2 \right), \quad (4)$$

$$M(x, t) - \mu \frac{\partial^2 M(x, t)}{\partial x^2} = EI \frac{\partial^2 v(x, t)}{\partial x^2}, \quad (5)$$

$I$  represents the second moment of area of the cross sections about axis  $z$ .

From the dynamic equilibrium of an infinitesimal element (Fig. 1(b)), in the longitudinal direction, one has

$$\frac{\partial N(x, t)}{\partial x} + f_u(x, t) = \rho A \frac{\partial^2 u(x, t)}{\partial t^2}, \quad (6)$$

where  $f_u(x, t)$  represents a distributed, longitudinal, external force.

From the dynamic equilibrium in the transverse direction and from the equilibrium of moments, one obtains

$$\begin{aligned} \frac{\partial^2 M(x, t)}{\partial x^2} - \frac{\partial}{\partial x} \left( N(x, t) \frac{\partial v(x, t)}{\partial x} \right) - f_v(x, t) \\ = - \rho A \frac{\partial^2 v(x, t)}{\partial t^2} + \rho I_z \frac{\partial^4 v(x, t)}{\partial x^2 \partial t^2}. \end{aligned} \quad (7)$$

Eqs. (6) and (7) are classical dynamic equilibrium equations, which are also applicable in the present non-local formulation [40].

Neglecting the longitudinal inertia and external longitudinal forces, it results from Eq. (6) that  $N(x, t)$  is constant along the CNT (nevertheless, we will keep argument  $x$ ) and Eq. (4) leads to

$$N(x, t) = EA \left( \frac{\partial u(x, t)}{\partial x} + \frac{1}{2} \left( \frac{\partial v(x, t)}{\partial x} \right)^2 \right), \quad (8)$$

with

$$EA \frac{\partial}{\partial x} \left( \frac{\partial u(x, t)}{\partial x} + \frac{1}{2} \left( \frac{\partial v(x, t)}{\partial x} \right)^2 \right) = 0. \quad (9)$$

Although it would be possible to obtain an expression for  $N(x, t)$  only as a function of the transverse displacement at this stage [43], this will not be done here, in order to arrive at equations of motion that directly follow – with addition of new terms – from the equations which were obtained in a work closely related with the current one, presented in reference [15], by application of the virtual work principle.

From (5) and (7), one arrives at the following expression for the bending moment

$$\begin{aligned} M(x, t) = EI \frac{\partial^2 v(x, t)}{\partial x^2} \\ + \mu \left( -\rho A \frac{\partial^2 v(x, t)}{\partial t^2} + \frac{\partial}{\partial x} \left( N(x, t) \frac{\partial v(x, t)}{\partial x} \right) + f_v(x, t) \right). \end{aligned} \quad (10)$$

From Eqs. (7) and (10) we deduce that

$$\begin{aligned} \rho A \left( \frac{\partial^2 v(x, t)}{\partial t^2} - \mu \frac{\partial^4 v(x, t)}{\partial x^2 \partial t^2} \right) + EI \frac{\partial^4 v(x, t)}{\partial x^4} \\ + \mu \frac{\partial^3}{\partial x^3} \left( N(x, t) \frac{\partial v(x, t)}{\partial x} \right) - \frac{\partial}{\partial x} \left( N(x, t) \frac{\partial v(x, t)}{\partial x} \right) \\ = f_v(x, t) - \mu \frac{\partial^2 f_v(x, t)}{\partial x^2}. \end{aligned} \quad (11)$$

In terms of displacement components, the partial differential equations of motion are Eqs. (9) and (11), with  $N(x, t)$  given by (8).

In the present study, transverse force  $f_v(x, t)$  is an electrostatic distributed force represented as  $f_e(x, t)$ . In [26,44] the electrostatic force per unit length of the nanotube is obtained by differentiating the electrostatic potential energy; the charge distribution of a finite length nanotube is first modelled with uniform charge distribution corresponding to an infinitely long, perfectly conductive cylindrical nanotube, placed over an infinite conducting plane, but then the expression is altered to consider the effect of concentrated charges at clamped and free ends. However, “the effect of charges present at the clamped end on the deflection of the nanotube is quite limited”, so only concentrated charges at the free end affect the expression of the electrostatic force [38,39]. Since the case studies of the present paper do not include free ends, we will adopt the expression given in [26] for the electrostatic force without considering the concentrated charge at the ends. Then the electrostatic force on the CNT is:

$$\begin{aligned} f_e(x, t) \\ = - \frac{\pi \epsilon_0 V^2}{d} \\ \frac{1}{\sqrt{\left( 1 + \frac{v(x, t)}{d} \right) \left( 1 + \frac{v(x, t)}{d} + 2 \frac{R_{ext}}{d} \right) \operatorname{arccosh}^2 \left( 1 + \frac{(1 + v(x, t)/d)}{R_{ext}/d} \right)}} \end{aligned} \quad (12)$$

In Eq. (12),  $\epsilon_0$  is the permittivity of free space, the other symbols were already defined. We will assume that the resonator is in a vacuum and that dissipation forces are negligible. In addition to the previously mentioned references [26,44], the same or similar expressions for the electrostatic force in CNTs have been derived in [25] and applied in a few works, including [8,27].

At the scales of interest in this paper, one might contemplate the consideration of Van der Waals forces. However, it was shown in [27] that, in the case of clamped-clamped boundaries, the electrostatic forces dominate the Van der Waals interactions; in that work, only for smaller gaps did the Van der Waals forces become meaningful. Furthermore, in [25] static deflection and pull-in were investigated on a clamped-clamped CNT with length 50 nm, diameter 2 nm and a gap of 4 nm; it was found that the effect of Van der Waals forces is negligible (it was also found that the same is not true when one boundary is clamped and the other free). In a case study performed in [8], Van der Waals forces were found to have a very small effect on clamped-clamped a CNT, when the gap width was 3 nm. Only clamped-clamped CNTs are considered in this paper and very small gap widths will not be considered: Van der Waals forces will be neglected.

## 2.2. Taylor expansion of external force

The equations of motion will be solved by the harmonic balance method, and, for that purpose, it is convenient that the external force has a polynomial form. Moreover, the polynomial form also turns easier the application of Galerkin's method, avoiding integrals where shape functions appear in a square root and in inverse hyperbolic cosine functions, both of which are in the denominator in Eq. (12). Hence, the electrostatic force given by Eq. (12) is approximated by its truncated Taylor series around  $v(x, t)=0$ . This Taylor expansion of the electrostatic force about  $v(x, t)=0$  can be written as

$$f_e(x, t) = -\pi\varepsilon_0 V^2 \left( \sum_{i=0}^n T_i^{fe}(d, R_{ext}) v(x, t)^i + o(v(x, t)^{n+1}) \right) \quad (13)$$

$o(v^{n+1})$  represents terms of  $n+1$  and higher orders in  $v$ . The expressions of the terms of the truncated Taylor series, terms  $T_i^{fe}(d, R_{ext})$ , are not included here, because even the lower order ones are far too long. The accuracy of diverse truncations is discussed in Section 3.1. We wish to study free vibrations, therefore, the voltage applied between the electrodes, represented by letter  $V$ , is constant (in other words, there is only a DC component).

## 2.3. Ordinary differential equations of motion

A  $p$ -version type approach is followed in this work, so we now derive the matrices associated with one finite element. Non-dimensional coordinate  $\xi$  is employed instead of  $x$ ; in our case  $\xi$  goes from  $-1$  to  $1$ . If axis  $x$  and  $\xi$  are aligned, the relation between the global ( $x$ ) and the local ( $\xi$ ) coordinates is  $x = x_i + \Delta x_i/2 + \xi \Delta x_i/2$ , with  $x_i$  the location of the left node of element number  $i$  and  $\Delta x_i$  the element length. To represent a single CNT, one  $p$ -version element is sufficient [15,45]; therefore, in this paper  $\Delta x_i=L$  and, when deriving the generalised force vector, the stiffness matrices and the mass matrices corresponding to one element, we are also deriving the matrices and generalised force vector of the final equation of motion.

The displacement components are written as

$$\begin{Bmatrix} u(\xi, t) \\ v(\xi, t) \end{Bmatrix} = \begin{Bmatrix} \mathbf{f}_u(\xi)^T & \mathbf{0} \\ \mathbf{0} & \mathbf{f}_v(\xi)^T \end{Bmatrix} \begin{Bmatrix} \mathbf{q}_u(t) \\ \mathbf{q}_v(t) \end{Bmatrix}, \quad (14)$$

where  $\mathbf{q}_u(t)$  and  $\mathbf{q}_v(t)$  are generalised displacement vectors, known as generalised coordinates in Lagrangian mechanics. Two vectors of shape functions are visible on equation (14):  $\mathbf{f}_u(\xi)$  and  $\mathbf{f}_v(\xi)$ . The former is constituted by linear functions plus a set of functions designated as  $g$  functions in [15,46,47]; the latter is in general constituted by cubic polynomials plus the set of  $f$  functions – often designated as polynomials in of Legendre in Rodrigues' form – presented for example in [47,48]. For the sake of completeness, the expressions of the higher order shape functions are provided here:

$$g_r(\xi) = \sum_{n=0}^{\text{INT}(r/2)} \frac{(-1)^n (2r - 2n - 5)!!}{2^n n! (r - 2n - 1)!} \xi^{r-2n-1}, \quad r > 2. \quad (15)$$

$$f_r(\xi) = \sum_{n=0}^{\text{INT}(r/2)} \frac{(-1)^n (2r - 2n - 7)!!}{2^n n! (r - 2n - 1)!} \xi^{r-2n-1}, \quad r > 4. \quad (16)$$

In the former expressions,  $r! = r(r-2) \dots (2 \text{ or } 1), 0! = (-1)!$   $= 1$  and  $\text{INT}(r/2)$  denotes the integer part of  $r/2$ . In reference [47] these shape functions are compared with other polynomial and non-polynomial shape functions. Instead of cubic polynomials plus functions  $f_r(\xi)$ , one may use functions  $g_r(\xi)$  for displacement components  $v(x, t)$  when the boundaries are hinged-hinged.

To improve the approximation, the number of shape functions and generalised coordinates is increased, increasing the dimension of vectors in (14).

Expression (13) is inserted in the partial differential equation of motion (11), and this equation is multiplied by the transverse shape functions (components of  $\mathbf{f}_v(\xi)$ ). Then the equations are integrated by parts in the domain leading to a set of ordinary differential equations of motion, which can be written as follows

$$\begin{aligned} & [\mathbf{M}_v + \mathbf{M}_{\mu v}] \ddot{\mathbf{q}}_v(t) + [\mathbf{K}_v^0 + \mathbf{K}_{fe}^0 + \mathbf{K}_{\mu fe}^0] \dot{\mathbf{q}}_v(t) \\ & + [2\mathbf{K}_{uv}^1(\mathbf{q}_v(t)) + \mathbf{K}_{\mu uv}^1(\mathbf{q}_v(t))] \mathbf{q}_u(t) + [\mathbf{K}_v^2(\mathbf{q}_v(t)) \\ & + \mathbf{K}_{\mu v}^2(\mathbf{q}_v(t)) + \mathbf{K}_{fe}^1(\mathbf{q}_v(t)) + \mathbf{K}_{fe}^2(\mathbf{q}_v(t)) + \mathbf{K}_{fe}^3(\mathbf{q}_v(t))] \\ & + [\mathbf{K}_{\mu fe}^1(\mathbf{q}_v(t)) + \mathbf{K}_{\mu fe}^2(\mathbf{q}_v(t)) + \mathbf{K}_{\mu fe}^3(\mathbf{q}_v(t))] \mathbf{q}_v(t) + \mathbf{v}_{fe} = \mathbf{0} \end{aligned} \quad (17)$$

$\mathbf{M}_v$  is the local mass matrix associated with the transverse acceleration [15];  $\mathbf{M}_{\mu v}$  is a mass matrix due to the effects of transverse inertia on the non-local part of the bending moment [45]. In the stiffness matrices, numbers in superscript correspond to the dependence of the matrices on the transverse generalised displacements in the following way: number 0 indicates that the matrix is constant; number 1 indicates that the matrix is a linear function of the transverse displacements  $\mathbf{q}_v(t)$ , 2 indicates a quadratic dependence and 3 a cubic. The letters in subscript indicate the displacements, non-local or electrostatic effects that are related with the respective matrix. Matrix  $\mathbf{K}_v^0$  is the constant stiffness matrix due to bending; matrix  $\mathbf{K}_{uv}^1(\mathbf{q}_v(t))$  is a matrix due to coupling between the longitudinal and the transverse displacement components and depends linearly on  $\mathbf{q}_v(t)$ ; matrix  $\mathbf{K}_v^2(\mathbf{q}_v(t))$  depends quadratically on  $\mathbf{q}_v(t)$  and is due to the transverse displacement and to the consideration of large displacements (from Von Kármán strains). The former stiffness matrices are given in [15].

Stiffness matrices  $\mathbf{K}_{\mu uv}^1(\mathbf{q}_v(t))$  and  $\mathbf{K}_{\mu v}^2(\mathbf{q}_v(t))$  are due to the non-local and geometrically non-linear effects. They were given in [45].

The following vector and matrices are due to the electrostatic force:

$$\mathbf{v}_{fe} = \frac{\pi\varepsilon_0 V^2 L}{2} T_0^{fe}(d, R_{ext}) \int_{-1}^1 \mathbf{f}(\xi) d\xi \quad (18)$$

$$\mathbf{K}_{fe}^0 = \frac{\pi\varepsilon_0 V^2 L}{2} T_1^{fe}(d, R_{ext}) \int_{-1}^1 \mathbf{f}(\xi) \mathbf{f}^T(\xi) d\xi \quad (19)$$

$$\mathbf{K}_{fe}^1(\mathbf{q}_v(t)) = \frac{\pi\varepsilon_0 V^2 L}{2} T_2^{fe}(d, R_{ext}) \int_{-1}^1 \mathbf{f}(\xi) \mathbf{f}^T(\xi) (\mathbf{f}^T(\xi) \mathbf{q}_v(t)) d\xi \quad (20)$$

$$\mathbf{K}_{fe}^2(\mathbf{q}_v(t)) = \frac{\pi\varepsilon_0 V^2 L}{2} T_3^{fe}(d, R_{ext}) \int_{-1}^1 \mathbf{f}(\xi) \mathbf{f}^T(\xi) (\mathbf{f}^T(\xi) \mathbf{q}_v(t))^2 d\xi \quad (21)$$

$$\mathbf{K}_{fe}^3(\mathbf{q}_v(t)) = \frac{\pi\varepsilon_0 V^2 L}{2} T_4^{fe}(d, R_{ext}) \int_{-1}^1 \mathbf{f}(\xi) \mathbf{f}^T(\xi) (\mathbf{f}^T(\xi) \mathbf{q}_v(t))^3 d\xi \quad (22)$$

Hence, after being expanded in a Taylor series until fourth order, the electrostatic force originates a constant vector  $\mathbf{v}_{fe}$ , and, due to the oscillations of the CNT, four matrices. Matrix  $\mathbf{K}_{fe}^0$  is constant, matrix  $\mathbf{K}_{fe}^1(\mathbf{q}_v(t))$  is a linear function of the generalised displacements  $\mathbf{q}_v(t)$ , matrix  $\mathbf{K}_{fe}^2(\mathbf{q}_v(t))$  is a quadratic function of  $\mathbf{q}_v(t)$  and matrix  $\mathbf{K}_{fe}^3(\mathbf{q}_v(t))$  a cubic function of  $\mathbf{q}_v(t)$ .

The non-local effects of the electrostatic force also originate a few matrices; to see those, we first go back to the Galerkin procedure. Multiplying  $\mu \frac{\partial^2 f_v(x, t)}{\partial x^2}$  by shape function  $f_i(x)$ , transforming to local coordinate  $\xi$ , integrating by parts and considering boundaries that preclude transverse displacements, we have

**Table 1**  
Geometrical and material properties of the CNTs studied in Section 3.1.

Case	$d$ (nm)	$L$ (nm)	$R_{ext}$ (nm)	$E$ (TPa)	$e_0 d/L$	Ref.
1	100	3000	30	1	0	[8]
2	3	20.7	0.68	–	0	[53]
3	4	50	0.6785	1	0–0.5	[27]

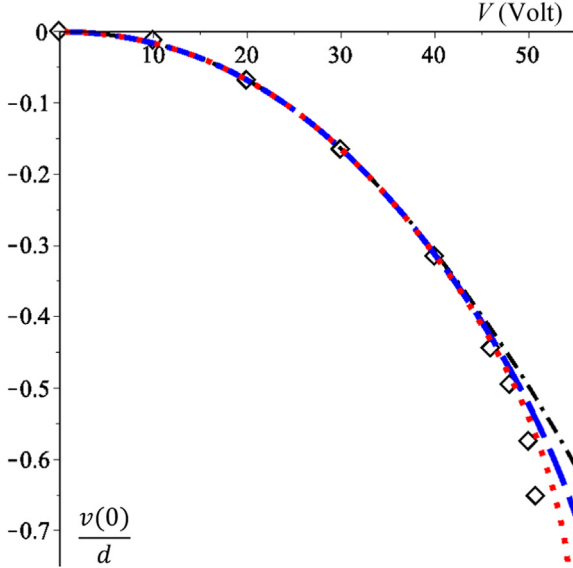


**Fig. 2.** Variation of static deflection of CNT with DC voltage, case 1 of Table 1; number of terms in Taylor series (equation (13)):  $n=3$ ,  $n=4$ ,  $n=5$ . Data from [8] is represented by  $\diamond$ . The numbers of transversal and longitudinal shape functions are, respectively:  $p_o=9$ ,  $p_l=12$ .

$$\int_{-1}^1 \mu \frac{2}{L} f_i(\xi) \frac{\partial^2 f_e(\xi, t)}{\partial \xi^2} d\xi = - \int_{-1}^1 \mu \frac{2}{L} \frac{\partial f_i(\xi)}{\partial \xi} \frac{\partial f_e(\xi, t)}{\partial \xi} d\xi \quad (23)$$

From Eq. (13), the Taylor expansion of  $\frac{\partial f_e(\xi, t)}{\partial \xi}$  is

$$\frac{\partial f_e(\xi, t)}{\partial \xi} = -\pi \epsilon_0 V^2 \left( \sum_{i=1}^n i T_i^{f_e}(d, R_{ext}) \frac{\partial v(\xi, t)^i}{\partial \xi} + o(v(x, t)^{n+1}) \right) \quad (24)$$

Inserting the terms of (24) into (23), the following matrices result:

$$\mathbf{K}_{\mu f_e}^0 = \frac{2\pi\mu\epsilon_0 V^2}{L} T_1^{f_e}(d, R_{ext}) \int_{-1}^1 \frac{\partial \mathbf{f}(\xi)}{\partial \xi} \frac{\partial \mathbf{f}^T(\xi)}{\partial \xi} d\xi \quad (25)$$

$$\mathbf{K}_{\mu f_e}^1(\mathbf{q}_v(t)) = \frac{4\pi\mu\epsilon_0 V^2}{L} T_2^{f_e}(d, R_{ext}) \int_{-1}^1 \frac{\partial \mathbf{f}(\xi)}{\partial \xi} \frac{\partial \mathbf{f}^T(\xi)}{\partial \xi} (\mathbf{f}^T(\xi) \mathbf{q}_v(t)) d\xi \quad (26)$$

$$\mathbf{K}_{\mu f_e}^2(\mathbf{q}_v(t)) = \frac{6\pi\mu\epsilon_0 V^2}{L} T_3^{f_e}(d, R_{ext}) \int_{-1}^1 \frac{\partial \mathbf{f}(\xi)}{\partial \xi} \frac{\partial \mathbf{f}^T(\xi)}{\partial \xi} (\mathbf{f}^T(\xi) \mathbf{q}_v(t))^2 d\xi \quad (27)$$

$$\mathbf{K}_{\mu f_e}^3(\mathbf{q}_v(t)) = \frac{8\pi\mu\epsilon_0 V^2}{L} T_4^{f_e}(d, R_{ext}) \int_{-1}^1 \frac{\partial \mathbf{f}(\xi)}{\partial \xi} \frac{\partial \mathbf{f}^T(\xi)}{\partial \xi} (\mathbf{f}^T(\xi) \mathbf{q}_v(t))^3 d\xi \quad (28)$$

Substituting in Eq. (9) the displacement components as given by (14) and applying Galerkin's method with longitudinal shape functions – components of vector  $\mathbf{f}_u(\xi)$  – as weight functions, an algebraic equation is derived. This equation can be solved to obtain the generalised displacements  $\mathbf{q}_u(t)$  as a function of  $\mathbf{q}_v(t)$ :

$$\mathbf{q}_u(t) = -\mathbf{K}_u^{-1} \mathbf{K}_{uv}^1(\mathbf{q}_v(t)) \mathbf{q}_v(t) \quad (29)$$

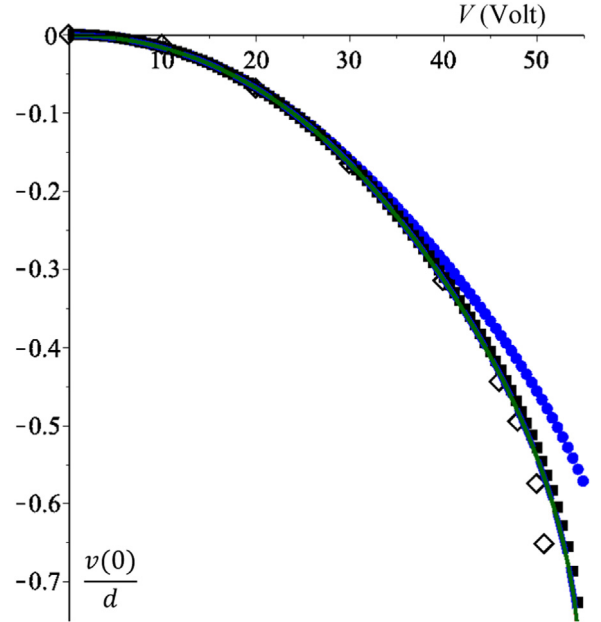


**Fig. 3.** Variation of static deflection of CNT with DC voltage, case 1 of Table 1; convergence with number of longitudinal shape functions ( $p_o=9$ ,  $n=5$ ):  $p_l=2$ ,  $p_l=4$ ,  $p_l=8$ ,  $p_l=12$ ,  $p_l=20$ . Data from [8] is represented by  $\diamond$ .

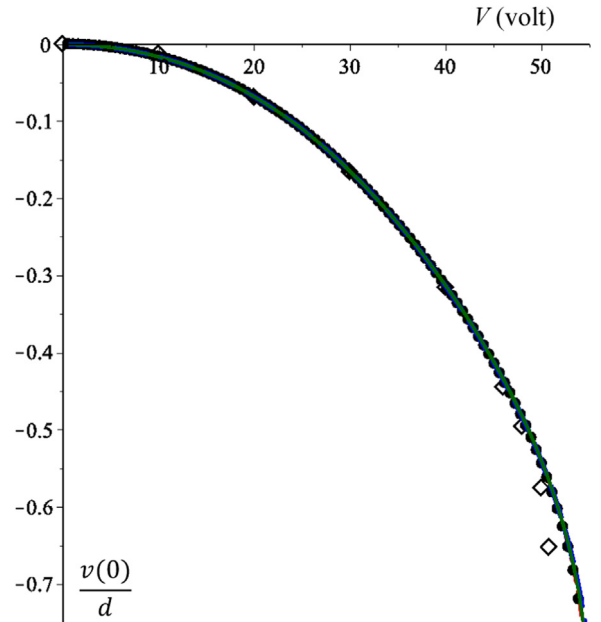


**Fig. 4.** Variation of static deflection of CNT with DC voltage, case 1 of Table 1; convergence with number of transverse shape functions ( $p_l=12$ ,  $n=5$ ):  $p_o=1$ ,  $p_o=3$ ,  $p_o=9$ ,  $p_o=12$ . Data from [8] is represented by  $\diamond$ .

Inserting the last expression in Eq. (17), leads to the following ordinary differential vector equation of motion in  $\mathbf{q}_v(t)$  only

$$\begin{aligned} & [\mathbf{M}_v + \mathbf{M}_{\mu v}] \ddot{\mathbf{q}}_v(t) + [\mathbf{K}_v^0 + \mathbf{K}_{f_e}^0 + \mathbf{K}_{\mu f_e}^0] \mathbf{q}_v(t) \\ & - [2\mathbf{K}_{uv}^T(\mathbf{q}_v(t)) + \mathbf{K}_{\mu uv}^1(\mathbf{q}_v(t))] \mathbf{K}_u^{0-1} \mathbf{K}_{uv}^1(\mathbf{q}_v(t)) \mathbf{q}_v(t) \\ & + [\mathbf{K}_v^2(\mathbf{q}_v(t)) + \mathbf{K}_{\mu v}^2(\mathbf{q}_v(t)) + \mathbf{K}_{f_e}^1(\mathbf{q}_v(t)) + \mathbf{K}_{f_e}^2(\mathbf{q}_v(t))] \\ & + [\mathbf{K}_{f_e}^3(\mathbf{q}_v(t)) + \mathbf{K}_{\mu f_e}^1(\mathbf{q}_v(t)) + \mathbf{K}_{\mu f_e}^2(\mathbf{q}_v(t)) + \mathbf{K}_{\mu f_e}^3(\mathbf{q}_v(t))] \mathbf{q}_v(t) \\ & + \mathbf{v}_{f_e} = \mathbf{0} \end{aligned} \quad (30)$$

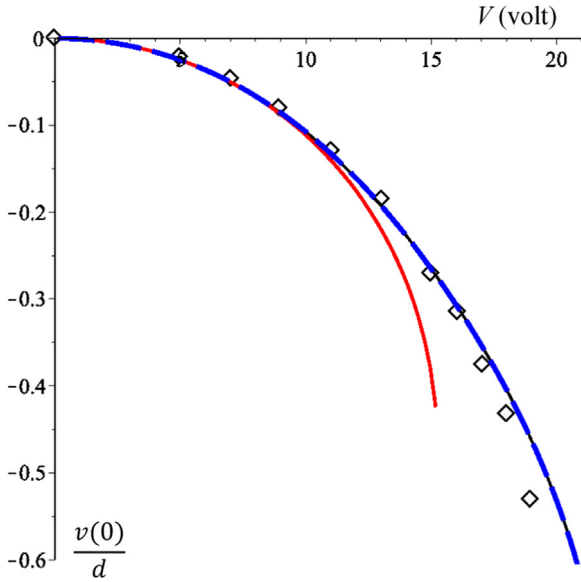


**Fig. 5.** Variation of static deflection of CNT with DC voltage, Case 2 of Table 1,  $n=5$ . Geometrically linear case, computed with  $p_o=7$ ,  $p_l=9$  and  $p_o=9$ ,  $p_l=20$  (coincident lines). Geometrically non-linear case, computed with  $p_o=7$ ,  $p_l=9$  and  $p_o=9$ ,  $p_l=20$  (coincident lines). The molecular dynamics results from [53] (read from a figure) are represented by  $\diamond$ .

There are non-linear terms of polynomial type up to the fourth degree and a constant vector in the equation of motion, a mathematical expression of the distinction between this and the cases of local [15] and non-local beams without electrostatic actuation [45], where the equations of motion are of the Duffing type (only cubic type non-linearities).

#### 2.4. Solution of the equations of motion

It is intended here to examine the combined effects of the non-local parameter and electrostatic force on the non-linear modes of vibration of CNT. We are only interested in periodic solutions of equations of motion (30), therefore, the solutions can be written in a Fourier series

$$\mathbf{q}_v(t) = \frac{\mathbf{u}_0}{2} + \sum_{i=1}^k (\mathbf{u}_i \cos(i\omega t)), \quad (31)$$

which is truncated to  $k+1$  terms. Vectors  $\mathbf{u}_i$  are the coefficients of the harmonics. In addition to one constant and to linear terms, the equations of motion contain odd and even polynomial type non-linear terms; for this reason, a constant term, odd and even harmonics are considered in (31). Because there are neither travelling waves, nor energy dissipation in the case at hand, sin terms are not required in the Fourier expansion (we are fixing the phase of each harmonic either to zero or  $\pi$ ).

Differentiating  $\mathbf{q}_v(t)$  twice with respect to time, and inserting  $\mathbf{q}_v(t)$  and  $\dot{\mathbf{q}}_v(t)$  in the equations of motion (30), we obtain equations that are not differential and contain sinusoidal functions of  $\omega t$ . Considering  $k=3$ , let's write them as

$$\mathbf{rf}_t(\mathbf{u}_0, \mathbf{u}_1, \mathbf{u}_2, \mathbf{u}_3, \omega, t) = \mathbf{0}, \quad (32)$$

To eliminate the cosines and time from Eq. (32), these equations are multiplied by each cosine and each product is integrated over one vibration period  $T$ :

$$\begin{aligned} \mathbf{rf}_{ci}(\mathbf{u}_0, \mathbf{u}_1, \mathbf{u}_2, \mathbf{u}_3, \omega) \\ = \frac{2}{T} \int_0^T \mathbf{rf}_t(\mathbf{u}_0, \mathbf{u}_1, \mathbf{u}_2, \mathbf{u}_3, \omega, t) \cos(i\omega t) dt, \quad i = 0 - 3, \end{aligned} \quad (33)$$

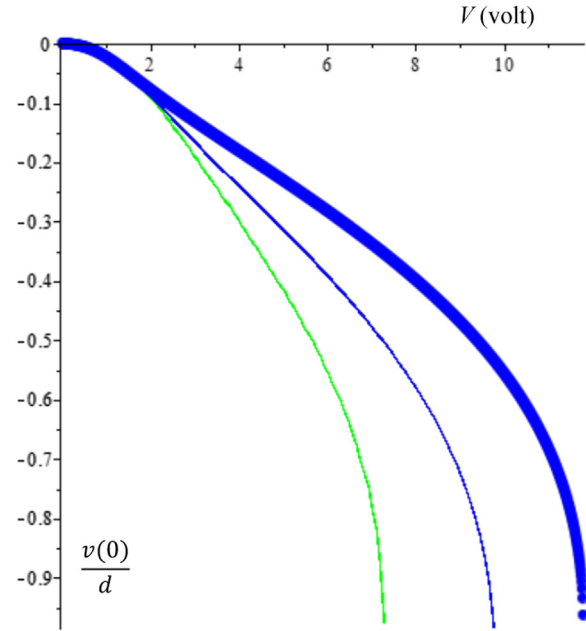


**Fig. 6.** Variation of static deflection of non-local CNT with DC voltage, Case 3 of.

taking advantage of the orthogonality of trigonometric functions. From this process – known as the harmonic balance method – a system of non-linear algebraic equations is obtained; it will be written as

$$\left\{ \begin{array}{l} -\omega^2 \begin{bmatrix} \mathbf{0} & \mathbf{0} & \mathbf{0} & \mathbf{0} \\ \mathbf{0} & \mathbf{M} & \mathbf{0} & \mathbf{0} \\ \mathbf{0} & \mathbf{0} & 4\mathbf{M} & \mathbf{0} \\ \mathbf{0} & \mathbf{0} & \mathbf{0} & 9\mathbf{M} \end{bmatrix} + \begin{bmatrix} \frac{1}{2}\mathbf{K}_e & \mathbf{0} & \mathbf{0} & \mathbf{0} \\ \mathbf{0} & \mathbf{K}_e & \mathbf{0} & \mathbf{0} \\ \mathbf{0} & \mathbf{0} & \mathbf{K}_e & \mathbf{0} \\ \mathbf{0} & \mathbf{0} & \mathbf{0} & \mathbf{K}_e \end{bmatrix} \end{array} \right\} \begin{Bmatrix} \mathbf{u}_0 \\ \mathbf{u}_1 \\ \mathbf{u}_2 \\ \mathbf{u}_3 \end{Bmatrix} \\ + \begin{Bmatrix} \mathbf{F}_0(\omega, \mathbf{u}_{HB}) \\ \mathbf{F}_1(\omega, \mathbf{u}_{HB}) \\ \mathbf{F}_2(\omega, \mathbf{u}_{HB}) \\ \mathbf{F}_3(\omega, \mathbf{u}_{HB}) \end{Bmatrix} = \begin{Bmatrix} -\mathbf{v}_{fe} \\ \mathbf{0} \\ \mathbf{0} \\ \mathbf{0} \end{Bmatrix}. \quad (34)$$

It results from (33) that each vector  $\mathbf{F}_i(\omega, \mathbf{u})$ ,  $i=1, 2, 3$ , in the former equation is given by

$$\mathbf{F}_i(\omega, \mathbf{u}_{HB}) = \frac{2}{T} \int_0^T \mathbf{K}_{n\ell}(\mathbf{q}(t)) \mathbf{q}(t) \cos(i\omega t) dt, \quad i = 1, 2, 3. \quad (35)$$

$\mathbf{F}_0(\omega, \mathbf{u}_{HB})$  is given by a similar expression, but divided by 2. Matrix  $\mathbf{K}_{n\ell}(\mathbf{q}(t))$  in (35) contains all matrices that give rise to non-linear terms in (30).

Separating the terms according to the order of the non-linearity, the frequency domain equations of motion (34) can be written as

$$\begin{aligned} (-\omega^2 \mathbf{M}_{HB} + \mathbf{K}_{eHB} + \mathbf{K}_{n\ell HB}^1(\mathbf{u}_{HB}) + \mathbf{K}_{n\ell HB}^2(\mathbf{u}_{HB}) + \mathbf{K}_{n\ell HB}^3(\mathbf{u}_{HB})) \mathbf{u}_{HB} \\ + \mathbf{R}_0 = \mathbf{0} \end{aligned} \quad (36)$$

The fundamental frequency of vibration  $\omega$  and the coefficients of each harmonic, which form vector  $\mathbf{u}_{HB}$ , are the unknowns of algebraic non-linear Eq. (36). In these equations, there are: a constant vector, represented by  $\mathbf{R}_0$ ; constant matrices,  $\mathbf{M}_{HB}$  and  $\mathbf{K}_{eHB}$ ; a matrix that depends linearly on  $\mathbf{u}_{HB}$ ,  $\mathbf{K}_{n\ell HB}^1(\mathbf{u}_{HB})$ ; a matrix that depends quadratically on  $\mathbf{u}_{HB}$ ,  $\mathbf{K}_{n\ell HB}^2(\mathbf{u}_{HB})$ ; a matrix that is a cubic function  $\mathbf{u}_{HB}$ ,  $\mathbf{K}_{n\ell HB}^3(\mathbf{u}_{HB})$ . In what concerns the application of the harmonic balance method, the constant vector, the mass

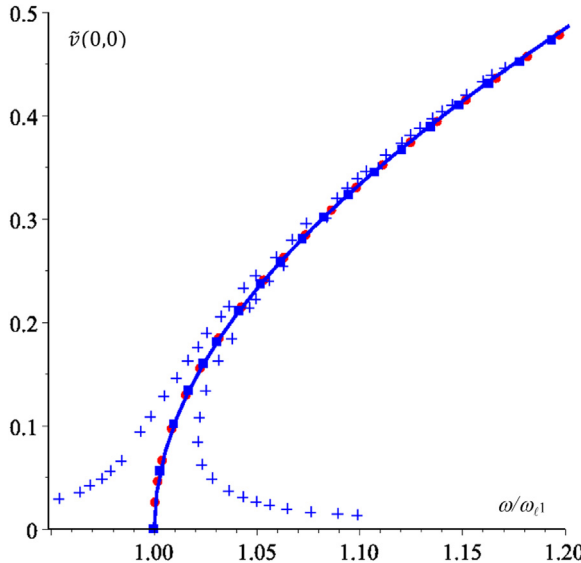


**Fig. 7.** Amplitudes of vibration computed with: ● one harmonic,  $p_o=p_l=5$ ; ■ one harmonic,  $p_o=6, p_l=8$ ; three harmonics,  $p_o=4, p_l=5$ . The points of the frequency response curve of Fig. 2, reference [54], are represented by +.

matrix  $\mathbf{M}_{HB}$ , and stiffness matrices up to (and including)  $\mathbf{K}_{nHB}^2(\mathbf{u}_{HB})$  have the form of matrices in [49,50]. Matrix  $\mathbf{K}_{nHB}^3(\mathbf{u}_{HB})$  is a novelty of this paper; its terms are very long and will not be written in detail.

The non-linear algebraic system of Eq. (36) is solved by an arc-length continuation method [51,52].

### 3. Numerical tests

#### 3.1. Convergence tests and comparisons

In this section, comparisons with results published by other authors are shown; furthermore, the convergence with the number of terms in the Taylor expansion of the electrostatic force (local and non-local parts), as well as the convergence with the number of shape functions, are analysed. It was difficult to find appropriate data for comparison in non-linear free vibrations and under the action of an electrostatic field, hence the comparisons now carried out are separated in two parts. The first set regards static deflections and the second set non-linear oscillations of the non-local CNT, but without electrostatic force. It should be added that the non-local model without electrostatic forces was also verified by comparison with other works in [45].

The geometric properties of the CNTs analysed are given in Table 1. The permittivity of free space,  $\epsilon_0$ , is for now – a value with more digits is introduced in the next section – made equal to  $8.854 \times 10^{-12}$  F/m, as in the references that serve for comparison. As written before, the length of the CNTs is represented by  $L$  and the external radius by  $R_{\text{ext}}$ . In the sources of Table 1, it was assumed that the tubes were full, therefore the effective tube thickness is  $h_t=R_{\text{ext}}$ . The CNTs are clamped at both ends.

In Fig. 2 the static deflection at the middle ( $x=0$ ) of a clamped-clamped carbon nanotube with the properties of Case 1 in Table 1 is shown. The deflection, represented by  $v(0)$ , is computed using Eq. (14), but without argument time, and is divided by the initial gap width. Nine transverse and twelve longitudinal shape functions were applied, i.e.,  $p_o=9, p_l=12$ . Convergence with the number of terms in the Taylor expansion of the electrostatic force, Eq. (13), is investigated and solutions from reference [8] are given

**Table 2**  
Properties of CNT analysed in Section 3.2.

Modulus of elasticity $E$ [TPa]	Mass density $\rho$ [ $\text{kg m}^{-3}$ ]	Non-local parameter $\epsilon_0 a$ [nm]	Effective tube thickness $h_t$ [nm]	Medium radius $r$ [nm]	Length $L$ [nm]
1.0	$1.3 \times 10^3$	0–5	0.34	0.4	50

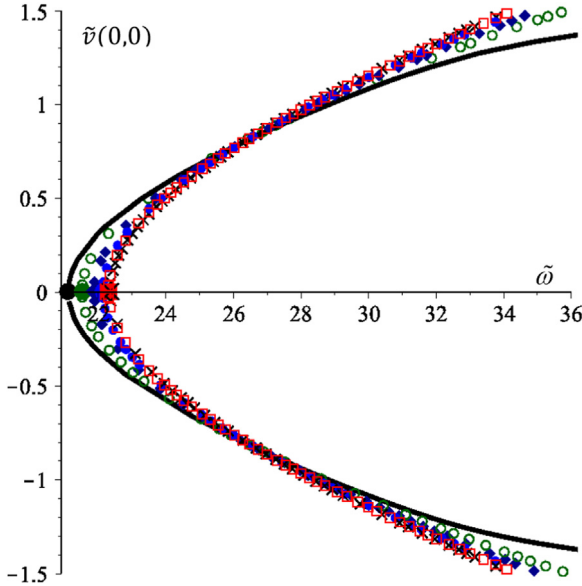
for comparison; the values were read from Fig. 2 of that reference and are therefore approximations. In reference [8], the CNT was modelled as a Bernoulli–Euler beam, Galerkin and Newton–Raphson methods were employed. The values of the diverse calculations are initially very close and increasingly deviate as the pull-in voltage is approached. The relative difference between the  $n=3$  and  $n=5$  approximations in the Taylor expansion (with the latter very close to reference [8]), when  $V=45$  V and  $v(0)/d \approx -0.4$ , is  $-3\%$ .

Fig. 3 illustrates the convergence with the number of longitudinal shape functions employed in Case 1 of Table 1. In this figure, all  $p$ -version results were computed with 9 transversal shape functions. At low vibration amplitudes, longitudinal shape functions are almost not required. But, naturally, as the vibration amplitude increases, so does the number of longitudinal shape functions necessary for accuracy, because the CNT stretches. In the range of amplitudes of Fig. 3 ( $|v(0)|/d < 0.8 \Rightarrow |v(0)|/(2R_{\text{ext}}) < 1.33(3)$ ), four longitudinal shape functions ( $p_l=4$ ) give quite accurate results; furthermore, whatever the magnitude of the displacement, the differences between computations with  $p_l=8, 12$  and  $20$  are not discernible (as explained at the end of this section, the true number of shape functions required is smaller, due to the symmetry of the problem).

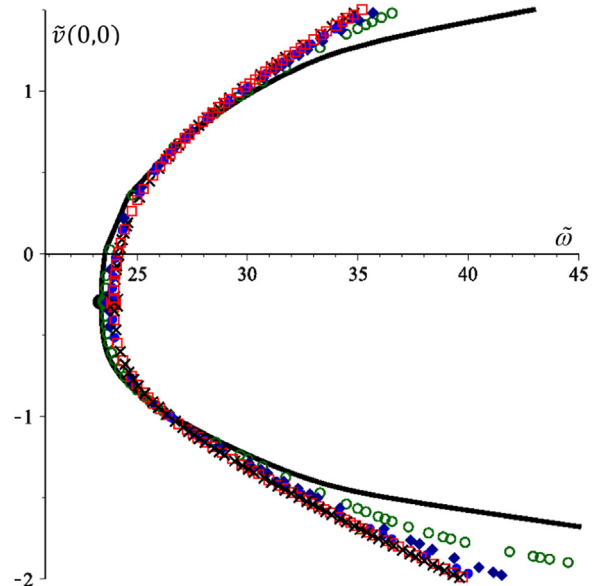
Still considering Case 1 of Table 1, Fig. 4 addresses the convergence with the number of transverse shape functions employed. In this figure, all  $p$ -version results were computed with 12 longitudinal shape functions ( $p_l=12$ , symmetric and anti-symmetric);  $p_o$  took values from 1 to 12 (also symmetric and anti-symmetric). In the range of amplitudes of Fig. 3 ( $|v(0)|/d < 0.8 \Rightarrow |v(0)|/(2R_{\text{ext}}) < 1.33(3)$ ), a  $p$ -element with one transverse shape function ( $p_o=1$ ) provides almost the same results as  $p$ -elements with more shape functions.

Fig. 5 provides a comparison between the displacement obtained in [53] via molecular dynamics and the one computed via the formulation presented here; the CNT has the properties of Case 2, Table 1. If geometrical non-linearity is disregarded, the values deviate from the geometrical non-linear ones as the displacement magnitude increases. With the scale employed in this figure, the difference between the geometrically linear and non-linear results becomes visible for  $|v(0)|/d > 0.1$ , which is approximately the same as  $|v(0)|/(2R_{\text{ext}}) > 0.22$ . The displacements computed with the present formulation are similar to the ones computed in [53] by molecular dynamics (MD), until  $V \approx 18.0$  V and  $v(0)/d \approx -0.432$ . Although not shown here, a continuum approach was also employed in [53], its results are, both in the geometrically linear case and in the geometrically non-linear case, closer to the ones of the present formulation than the MD results.  $P$ -version finite elements with  $p_o=7, p_l=9$  or with  $p_o=9, p_l=20$  were employed in Fig. 5; there is no visible difference between the results they originate. Five terms were used in Eq. (13), i.e.,  $n=5$ .

The last static example is taken from example from [27] and is presented in Fig. 6. In this example, non-local effects are taken into account; the properties are the ones of Case 3, Table 1. The results of the present approach were obtained assuming  $n=5$  in Eq. (13). The trend of the present results is similar to the one of the data



**Fig. 8.** Total amplitude of vibration displacement in the beginning of a vibration cycle versus natural frequency of vibration, when  $V=0$  V. The non-local parameter takes values:  $\times e_0a = 0$ ,  $\square e_0a = 1.0$  nm,  $\bullet e_0a = 2.0$  nm,  $\blacklozenge e_0a = 3$  nm,  $\circ e_0a = 4.0$  nm, —  $e_0a = 5.0$  nm.



**Fig. 10.** Total amplitude of vibration displacement in the beginning of a vibration cycle versus natural frequency of vibration, when  $V=2$  V. The non-local parameter takes values:  $\times e_0a = 0$ ,  $\square e_0a = 1.0$  nm,  $\bullet e_0a = 2.0$  nm,  $\blacklozenge e_0a = 3$  nm,  $\circ e_0a = 4.0$  nm, —  $e_0a = 5.0$  nm.

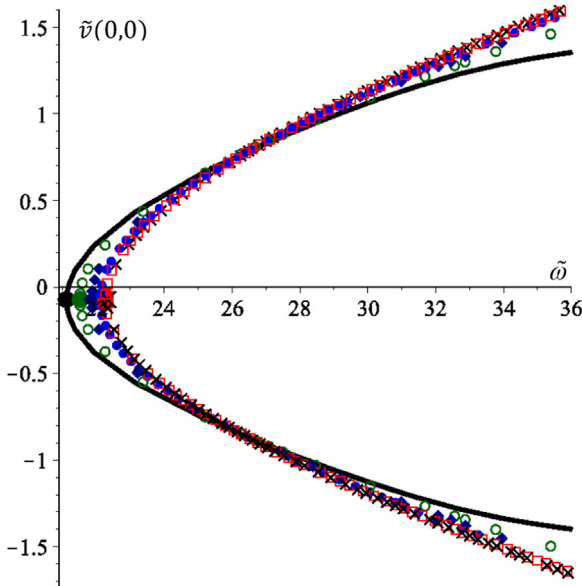


**Fig. 9.** Total amplitude of vibration displacement in the beginning of a vibration cycle versus natural frequency of vibration, when  $V=1$  V. The non-local parameter takes values:  $\times e_0a = 0$ ,  $\square e_0a = 1.0$  nm,  $\bullet e_0a = 2.0$  nm,  $\blacklozenge e_0a = 3$  nm,  $\circ e_0a = 4.0$  nm, —  $e_0a = 5.0$  nm.

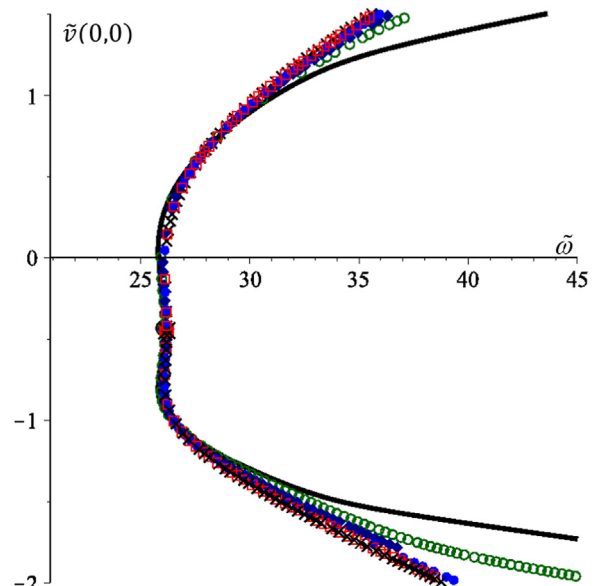


**Fig. 11.** Total amplitude of vibration displacement in the beginning of a vibration cycle versus natural frequency of vibration, when  $V=2.5$  V. The non-local parameter takes values:  $\times e_0a = 0$ ,  $\square e_0a = 1.0$  nm,  $\bullet e_0a = 2.0$  nm,  $\blacklozenge e_0a = 3$  nm,  $\circ e_0a = 4.0$  nm, —  $e_0a = 5.0$  nm.

presented in Fig. 4 of reference [27]: in both analyses, the larger the non-local parameter, the larger the voltage required to achieve a certain deflection. However, the values do not agree, not even in the local case ( $\mu=0$ ). Since the static local, electrostatic case was verified in the previous figures and since the natural frequencies of non-local problems computed with the present approach were accurately computed (Ref. [45] and an example that follows), we believe that the mathematical model and computational code developed in the framework of the present paper are correct, under the limitations explained along the derivation of the formulation.

Table 1, computed with  $p_0=7$ ,  $p_l=9$ . Local case,  $e_0a=0$ ,

represented by —, case  $e_0a/L=0.2$  represented by —; case  $e_0a/L=0.5$  represented by ●.

The comparisons performed in the previous paragraphs indicate that terms of order higher than the fourth ( $n \geq 5$ ) can be neglected with a small error in  $f_e(x, t)$  if  $|v(x, t)|/d| \leq 0.4$ . Furthermore, in order to investigate the accuracy and limitations of this Taylor expansion, the exact and the approximated expressions of non-dimensional term  $\frac{f_e(x, t)d}{\epsilon_0 b V^2}$  were plotted (plots not included here) for diverse values of  $R_{ext}/d$ . The relative difference between the function and its Taylor expansion with a small number of terms becomes larger as  $|v(x, t)|/d|$  increases, particularly if  $v$  is positive, but four terms provide a good approximation As a result

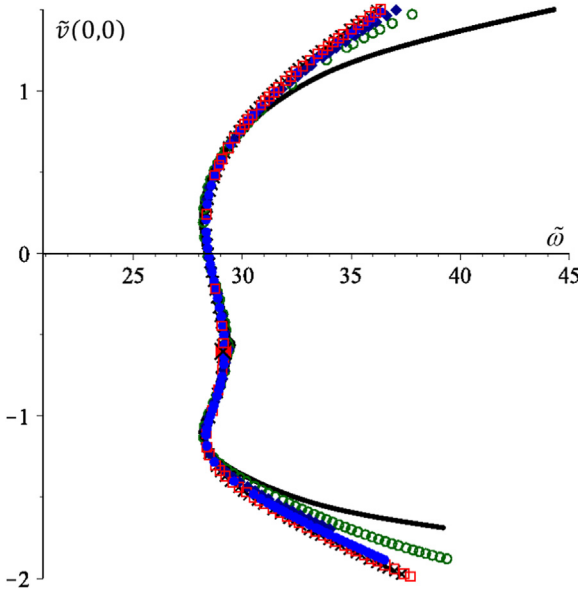


**Fig. 12.** Total amplitude of vibration displacement in the beginning of a vibration cycle versus natural frequency of vibration, when  $V=3$  V. The non-local parameter takes values:  $\times e_0a=0$ ,  $\square e_0a=1.0$  nm,  $\bullet e_0a=2.0$  nm,  $\blacklozenge e_0a=3$  nm,  $\circ e_0a=4.0$  nm, —  $e_0a=5.0$  nm.

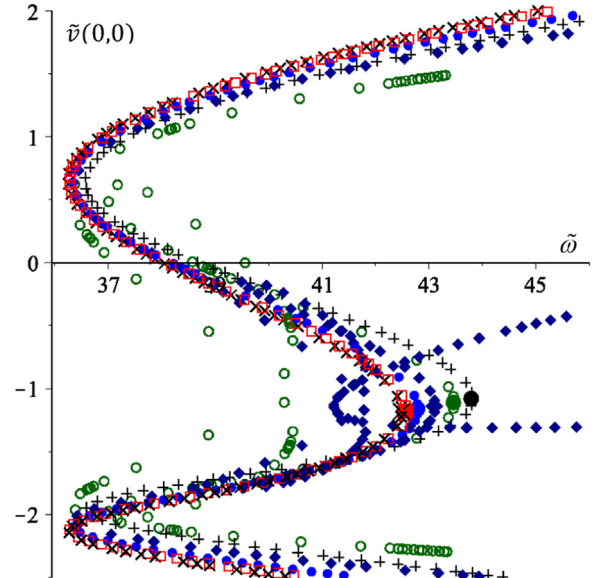


**Fig. 14.** Total amplitude of vibration displacement in the beginning of a vibration cycle versus natural frequency of vibration, when  $V=5$  V. The non-local parameter takes values:  $\times e_0a=0$ ,  $\square e_0a=1.0$  nm,  $\bullet e_0a=2.0$  nm,  $\blacklozenge e_0a=3$  nm,  $\circ e_0a=4.0$  nm, +  $e_0a=5.0$  nm.

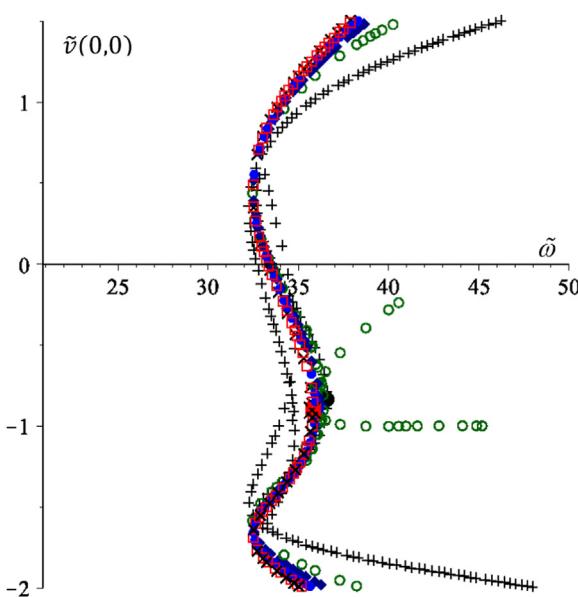


**Fig. 13.** Total amplitude of vibration displacement in the beginning of a vibration cycle versus natural frequency of vibration, when  $V=4$  V. The non-local parameter takes values:  $\times e_0a=0$ ,  $\square e_0a=1.0$  nm,  $\bullet e_0a=2.0$  nm,  $\blacklozenge e_0a=3$  nm,  $\circ e_0a=4.0$  nm, +  $e_0a=5.0$  nm.

of this conclusion,  $n=4$  in the vibration analysis that are presented in Section 3.2.2 and we will in general avoid cases where  $|v(x,t)|/d| > 0.4$  (exceptions occur in Fig. 14, where  $|v(x,t)|/d|$  achieves value 0.475).

It is important to stress that, in all the previous analyses, including in the studies of convergence with the number of shape functions, advantage was not taken of the symmetry of the problems. Therefore, the computational models are general, in the sense that they apply to symmetric and non-symmetric problems. But the true number of shape functions required for convergence in each of the specific cases analysed – cases which are all symmetric about axis  $y$  – is about half the one given.

The final test of this section addresses the natural frequencies

of vibration of a hinged-hinged, non-local CNT vibrating in the non-linear regime. The material and geometric properties are:  $E=1.1$  TPa,  $\rho=1300$  kg/m<sup>3</sup>,  $R_{\text{ext}}=3$  nm,  $h_t=0.34$  nm,  $L=40 R_{\text{ext}}$ . The non-local parameter  $e_0a$  is  $0.0333L$ . This case is taken from [54], where Galerkin method was employed to obtain the equations of motion and software AUTO was employed to solve those equations. Fig. 7 shows the non-dimensional amplitude (for details on its computation, see Section 3.2) as a function of the non-dimensional frequency. The fundamental natural frequency of the linear system is represented by  $\omega_{\parallel}$ . In [54], steady-state forced vibrations due to a harmonic force are computed originating a frequency response curve, for which  $\omega$  is the excitation frequency; in the free vibration results,  $\omega$  represents the natural frequency of vibration. Therefore, the present free vibration results should be in between the stable and unstable parts of the frequency response curve of [54]. A remarkable agreement exists between the present approach and reference [54].

Only symmetric transverse shape functions and antisymmetric longitudinal shape functions were employed to compute the data shown on Fig. 7. A full convergence study was not performed, but results from models with different numbers of shape functions are presented, in order to demonstrate that convergence has been achieved. Furthermore, in this case the backbone curve computed with one harmonic coincides with the backbone curve computed with the constant term and three harmonics.

### 3.2. Non-linear modes of vibration

This section is devoted to the analyses of the combined effects of electrostatic forces, non-locality and geometrical non-linearity on the non-linear modes of vibration of CNTs.

#### 3.2.1. Material, geometric and electrostatic force properties

In order to adopt geometric and mechanic properties that are somehow representative of real CNTs, a literature review was carried out. In reference [55], values for the Young modulus of CNT are obtained by analysing thermal vibrations and assuming that a carbon nanotube is a cantilever beam of hollow cylindrical cross section; Young's modulus from 0.40 TPa to 4.15 TPa are estimated; diverse values for lengths, inner and outer diameters of CNT are given. Wang

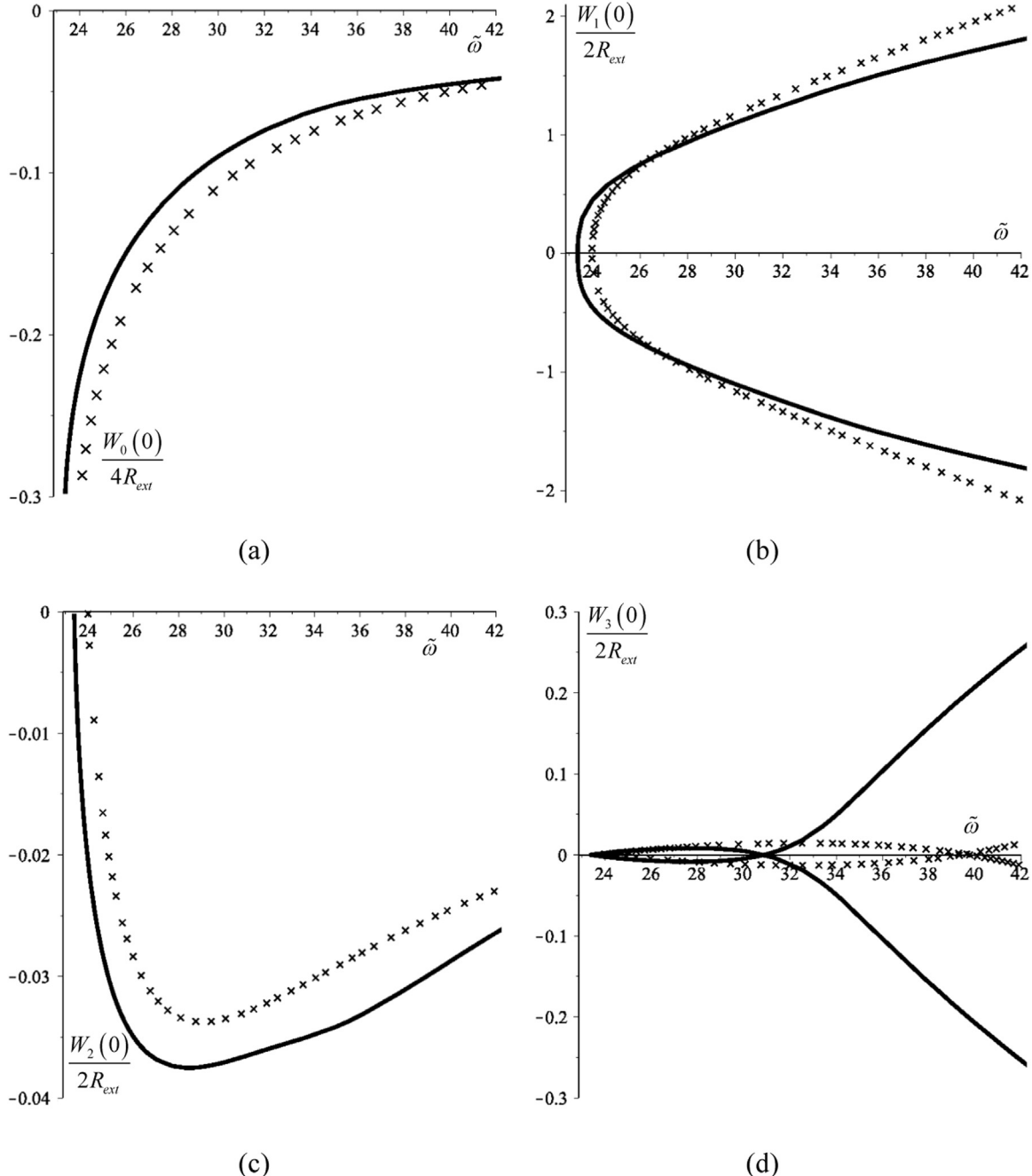


**Fig. 15.** Amplitudes of harmonics of the transverse vibration displacement, computed at  $x=0$ , when  $V=2$  V and the non-local parameter  $e_0a$  is either equal to 0 ( $\times$ ) or to 5.0 nm (—). Sub-figure (a) represents the magnitude of the constant term. The other sub-figures represent the amplitudes of the following harmonics: (b) first; (c) second; (d) third.

et al. [56] used transmission electron microscopy to carry out measurements of the mechanical properties on CNTs produced either by pyrolysis or by an arc-discharge technique. The modulus of Young varied substantially from one case to another (from a few GPa to 1.2 TPa). Diverse lengths, inner and outer diameters are again given. Yang et al. [39] estimated Young's modulus of CNT using Molecular Mechanics simulations; the values depended on the type of CNT, but were always slightly larger than 1.1 TPa. The authors also provide values for the geometric properties of CNT. C. Li and T.-W Chou [57] established a link between molecular mechanics and structural mechanics to arrive at Young's modulus for single walled CNTs that vary with the diameter and chirality of the tubes. Furthermore, it is assumed in [57] that the thickness of a single walled carbon nanotube is 0.34 nm, equal to the interlayer spacing of graphite. Xiao et al. [58]

also adopt an effective thickness equal to 0.34 nm and arrive at Young's modulus that are not far from  $E=1.0$  TPa. Both in [57,58], reference is made to experimental analyses that to some extent sustain the values obtained. In reference [59], value 1TPa is adopted for the modulus of Young, it is considered that the effective thickness of single-walled carbon nanotubes is 0.35 nm and that the mass density is  $1.3 \times 10^3$  kg/m<sup>3</sup>. Diverse values for Young's modulus of CNT are quoted in [60], including 1 TPa.

In what the non-local parameter  $e_0a$  is concerned, Wang [61] used the fundamental natural frequency of a CNT, experimentally identified to be around 0.1 THz in [62], to conclude that the non-local parameter of single-walled carbon nanotubes (SWCNTs) should be  $e_0a < 210$  nm. In the same paragraph, but following references according to which the measured frequency of SWNT is

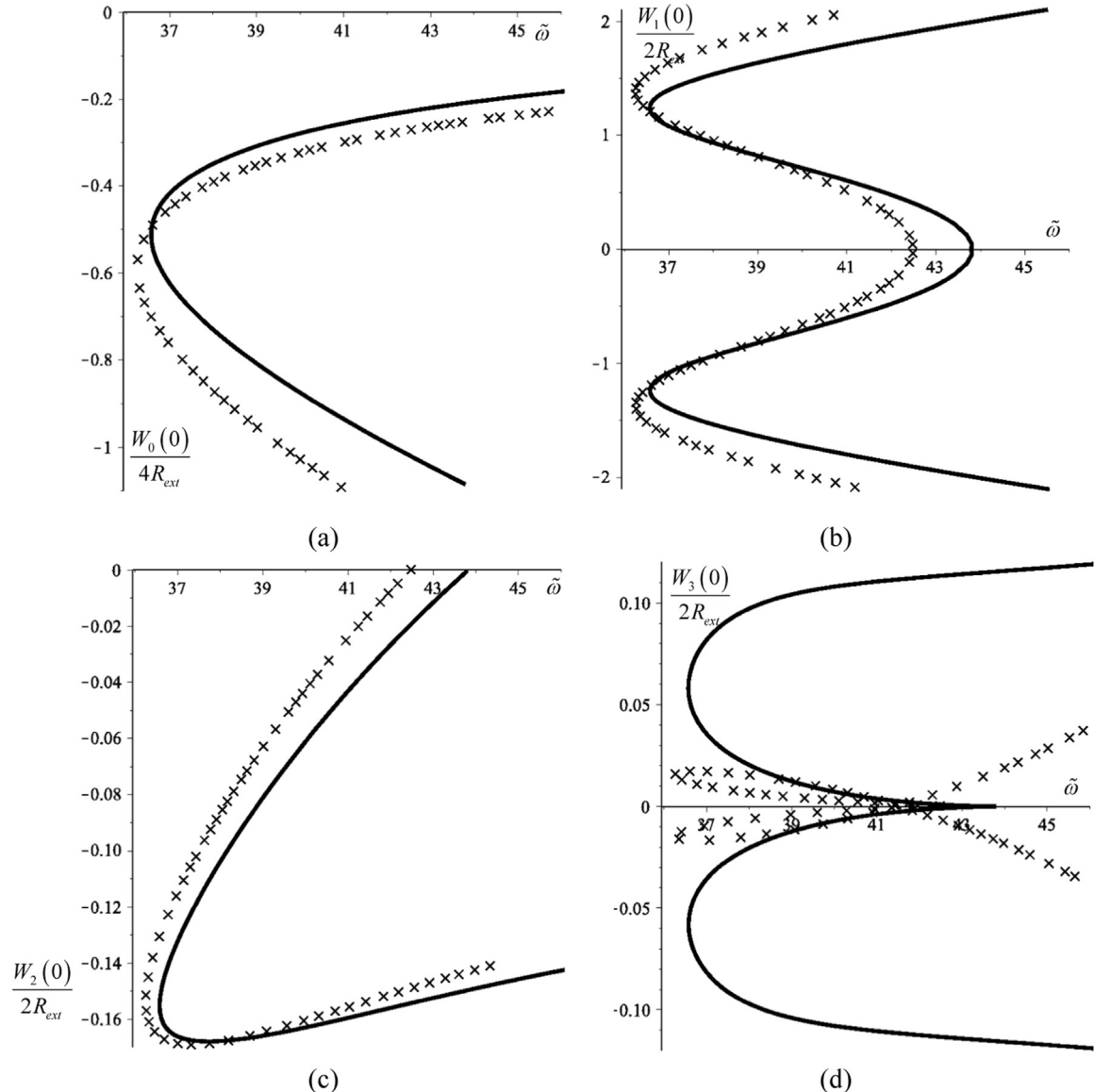


**Fig. 16.** Amplitudes of harmonics of the transverse vibration displacement, computed at  $x=0$ , when  $V=5$  V and the non-local parameter  $e_0a$  is either equal to 0 ( $\times$ ) or to 5.0 nm (—). Figure (a) represents the magnitude of the constant term. The other figures represent the amplitudes of the following harmonics: (b) first; (c) second; (d) third.

greater than 10 THz, the scale coefficient was deduced to be  $e_0a < 2.1$  nm. Şimşek [40] quotes [61] to justify adopting  $e_0a$  between 0 and 2 nm. The estimates of Wang [61] are also referred/adopted in [36].

In conclusion, a large range of values can be found for material and geometric properties of CNT in the literature. Taking the aforementioned publications as guidance, we can say that the values of [Table 2](#) are possible and will, from now on, adopt them. The radius given in [Table 2](#) is the mean radius,  $r = (R_{ext} - h_t/2)$ . Since there is some variability in the possible value of  $e_0a$ , and in order to investigate the scale effects, we will consider several values in the range  $0 < e_0a < 5.0$  nm. Furthermore, non-dimensional values of the non-local parameter and of the transverse displacement of the CNT will be provided. The non-dimensional non-local parameter is  $\zeta = e_0a/L$ . To obtain the non-dimensional transverse displacement, we divide the transverse displacement,  $v(x,t)$ , by the diameter of the CNT,  $2R_{ext}$ :

$$\tilde{v}(\xi, t) = \frac{v(\xi, t)}{2R_{\text{ext}}}. \quad (37)$$

With this non-dimensionalisation,  $\tilde{v}(\xi, t)$  gives us an indication of the importance of geometrical non-linear effects. The natural frequency of vibration is non-dimensionalised as well, applying the following equation,

$$\tilde{\omega} = \omega L^2 \sqrt{\frac{\rho A}{EI}}. \quad (38)$$

For the permittivity of free space,  $\epsilon_0$ , we will use  $8.854\ 187\ 82 \times 10^{-12}$  F/m (truncated from the value that is given in [63] with more significant digits). The initial distance between the electrode and the CNT,  $d$ , is 6 nm. The  $p$ -version finite elements employs 7 transverse and 10 longitudinal shape functions ( $p_o=7$ ,  $p_l=10$ ), or more. The DC voltage takes values between 0 V and 5 V.

### 3.2.2. Numerical tests

The non-linear modes of vibration of CNTs are now investigated, for several values of the electric potential  $V$  and of the non-local parameter  $e_0a$ . The former takes values 0, 1, 2, 2.5, 3, 4 and 5 V; the latter takes the following values (in nm)  $e_0a=0, 1, 2, 3, 4, 5$ , corresponding to a non-dimensional non-local parameter,

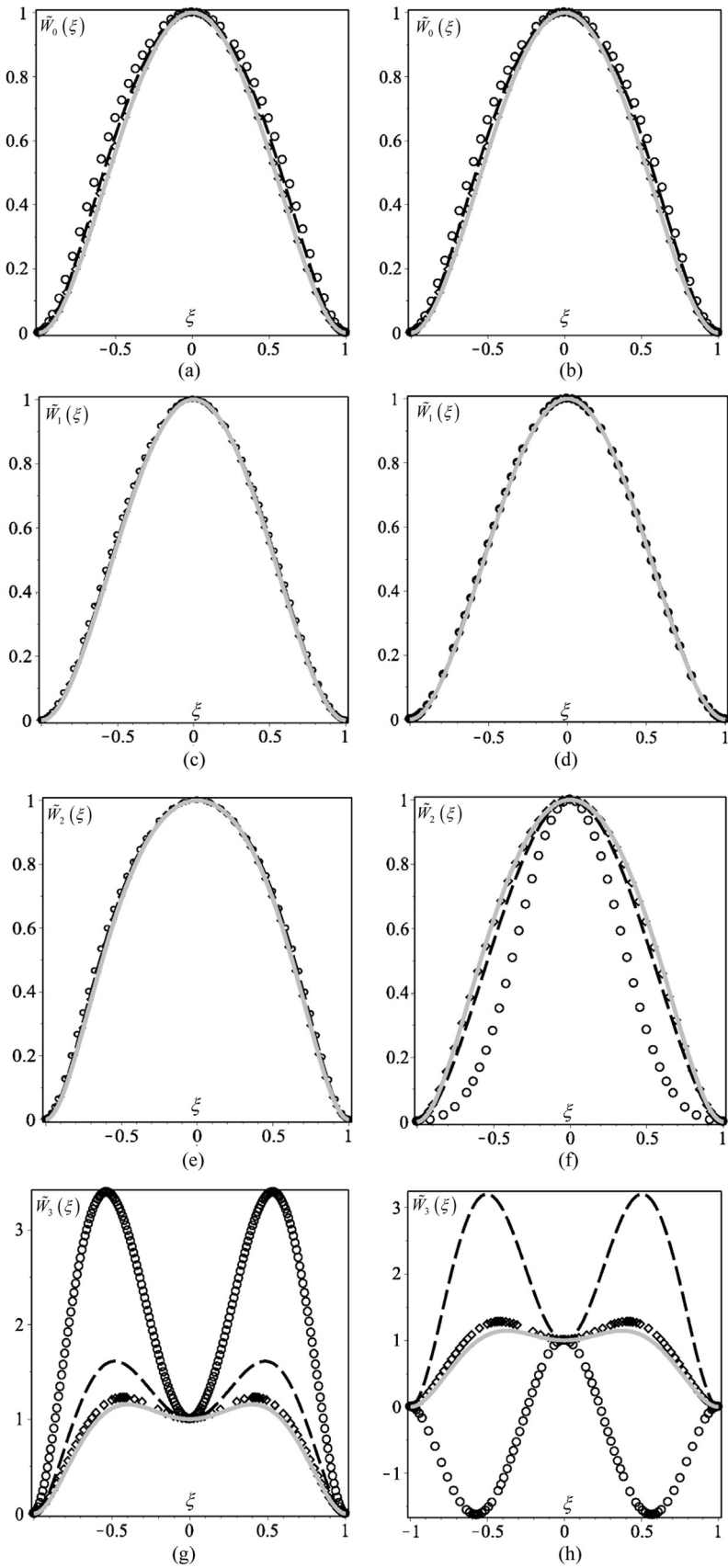


**Fig. 17.** Shapes of constant term – (a) and (b), first harmonic – (c) and (d), second harmonic – (e) and (f), third harmonic – (g) and (h), when  $V=2V$  and the non-local parameter,  $e_0a$ , is either equal to 0 (figures on the left) or to 5.0 nm (figures on the right). In each sub-figure, the shapes correspond to the following amplitudes of the first harmonic: —  $W_1(0)/(2R_{ext}) \approx 0$ ; ◇  $W_1(0)/(2R_{ext}) \approx 0.5$ ; —  $W_1(0)/(2R_{ext}) \approx 1.0$ ; ○  $W_1(0)/(2R_{ext}) \approx 1.5$ .

$\zeta$ , which is respectively equal to one of the following values: 0, 0.02, 0.04, 0.06, 0.08, 0.1. To turn the presentation clearer, this section is divided into three subsections, which address: backbone curves; shapes of vibration; time and phase plots.

**3.2.2.1. Backbone curves.** The variation of the natural frequency of vibration with the value of the non-dimensional transverse displacement in the beginning of an oscillation cycle,  $\tilde{v}(0, 0)$  is shown in Figs. 8–14, for the diverse cases. This non-dimensional transverse displacement is given by Eqs. (37), (14) and (31) with  $\xi=0$  and  $t=0$ . It was decided to show here this specific displacement because it provides an overall information; more detailed analysis of the modes of vibration, with exhibition of the diverse harmonics, will be performed after, in selected cases. The starting points of the backbone curves are marked in the figures by bigger dots. These points correspond to oscillations of infinitesimal amplitudes. In all except case  $V=0$  V, these oscillations occur about an equilibrium configuration where the CNT is deformed, i.e., the CNT is not straight.

Figs. 8–14 show that an increase of the voltage magnitude leads to an increase in the inward deflection of the CNT, which is associated with a deformed configuration about which oscillations occur. By increasing the amplitude of oscillations about this reference configuration, one only finds hardening spring effect when  $V=0$  V and  $V=1$  V. The difference between the curves defined when  $V=0$  V - Fig. 8 - and  $V=1$  V - Fig. 9 - is small; however, the offset caused by the electric potential is visible in the second case.

Voltage influences the dynamic behaviour of the CNT in a highly non-linear way; this becomes evident when  $V$  takes values greater or equal than 2 V. First (2 V, Fig. 10), the shapes markedly differ from the almost parabolic shapes of the 0 V and 1 V cases, portrayed in Fig. 8 and in Fig. 9; after ( $V>2$  V, Figs. 11–14), softening and turning points appear. Moreover, the complexity of the curves increases with  $V$ .

In Figs. 8–14 there are at least two values for the deflections at  $t=0$  s ( $\tilde{v}(0, 0)$ ) for a given frequency of vibration, one value for displacements in the positive direction and another for displacements in the negative direction. In the absence of electric potential, these values are symmetric, but they cease to be symmetric

when voltage exists. This is an interesting reflex of the asymmetry of the CNT electrostatically actuated on one side only, which will be better explained later on.

Non-local effects also have an influence on the modes of vibration of the electrostatically actuated CNTs. Let us first consider the natural frequency that corresponds to infinitesimal vibration amplitudes. This natural frequency is not designated as "linear natural frequency", because, with the exception of the 0 V case, the static component of the displacement is not zero, introducing geometrical non-linear effects. By increasing the voltage from zero to 5 V, a large increase is observed in the natural frequency that corresponds to an infinitesimally small vibration amplitude, because of the stiffening effect of the static component of the deformation of the CNT. For lower voltages, an increase in the non-local parameter decreases the aforementioned natural frequency of vibration. However, at about  $V=2.5$  V, changes in the non-local parameter barely affect that natural frequency. After, by further increasing the voltage, the larger the non-local parameter, the larger the natural frequency that corresponds to an infinitesimally small vibration amplitude. The dissimilar variation of the natural frequency under discussion in this paragraph with the non-local parameter is explained by the fact that the non-local effect influences this frequency in two opposite ways, related to terms visible in the partial differential Eq. (11) and in the ordinary differential Eq. (17). On the one hand, increasing the non-local effect, increases the effects of inertia forces, leading to a decrease in frequency (this is well-established, see, for example, references [41,45,64–66]). But, on the other hand, by increasing the non-local effect when the voltage has larger values, the amplitude of the static deflection diminishes and the natural frequency increases, because an increase in stiffness occurred, due to stiffness terms that only appear under the combination of non-local and geometrically non-linear effects. Another factor that is bound to influence the frequency at larger voltages is the non-local effect of the electrostatic force.

In what softening and hardening are concerned, it is obvious that when the voltage is 0, 1 or 2 V, the larger the non-local parameter, the larger the hardening spring effect. This is a consequence of the contribution of strains at all points in the domain to the stress at a particular point. The 0 V case was investigated in

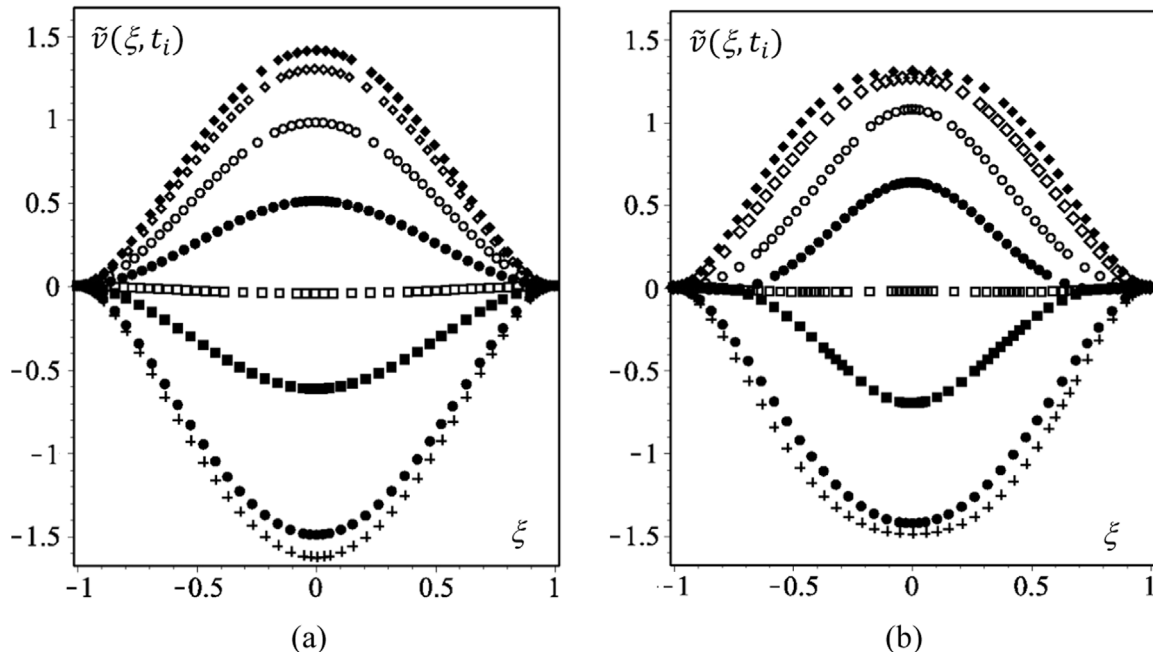


**Fig. 18.** Shapes of CNT at different instants along half a vibration period, with  $V=2$  V and (a)  $e_0a=0$ , (b)  $e_0a=5.0$  nm. In both cases the amplitude of the first harmonic is approximately equal to  $1.5 \times 2 R_{ext}$  ( $W_1(0)/(2 R_{ext}) \approx 1.5$ ). The shapes at  $t=0$  s are represented by symbol  $\blacklozenge$ , the shapes at  $t=T/2$  s are represented by symbol  $+$ .

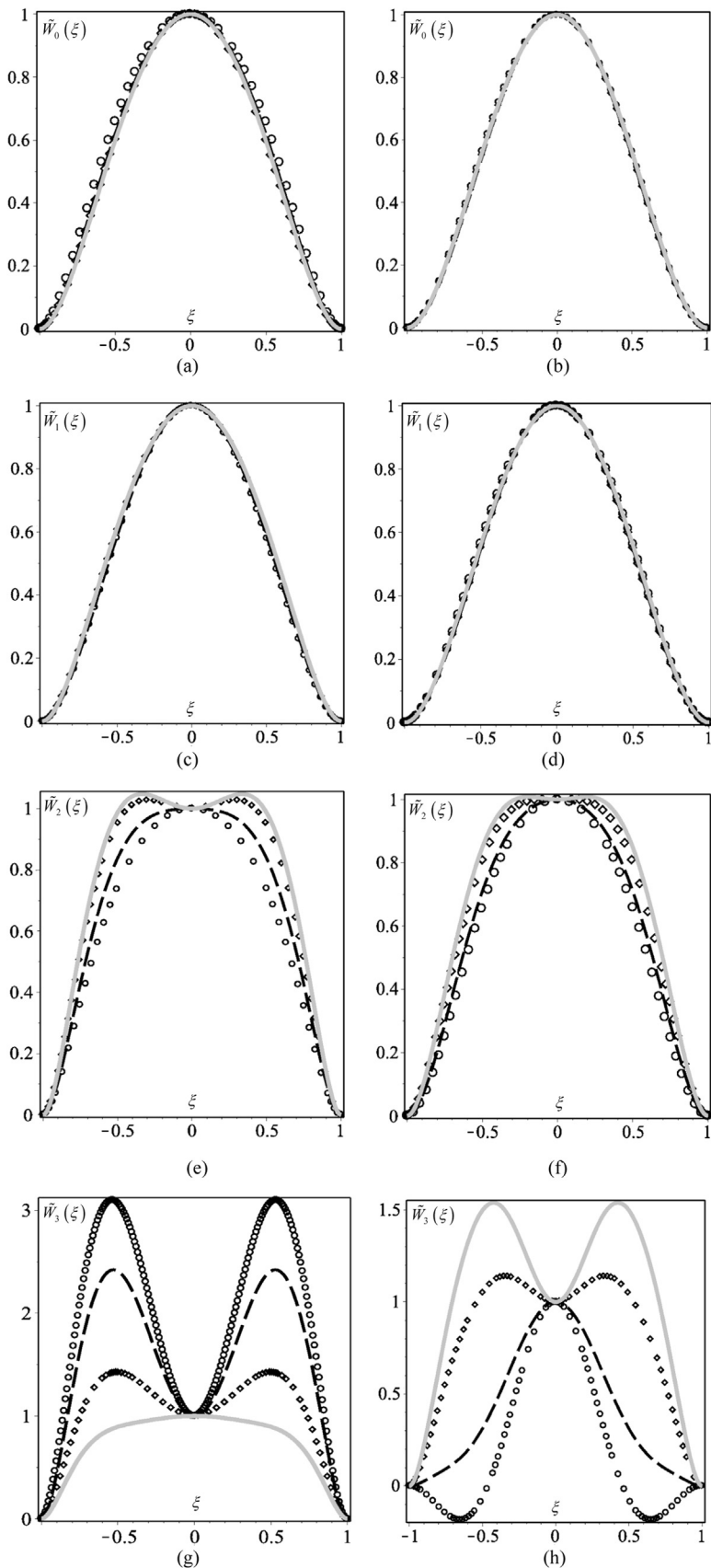


**Fig. 19.** Shapes of: (a) and (b) – constant term, (c) and (d) - first harmonic, (e) and (f) – second harmonic, (g) and (h) - third harmonic, when  $V=5$  V and the non-local parameter  $e_0a$  is either equal to 0 (figures on the left) or to 5.0 nm (figures on the right). In each sub-figure, the shapes correspond to the following amplitudes of the first harmonic: —  $W_1(0)/(2 R_{ext}) \cong 0$ ;  $\diamond W_1(0)/(2 R_{ext}) \cong 0.5$ ; —  $W_1(0)/(2 R_{ext}) \cong 1.0$ ;  $\circ W_1(0)/(2 R_{ext}) \cong 1.5$ .

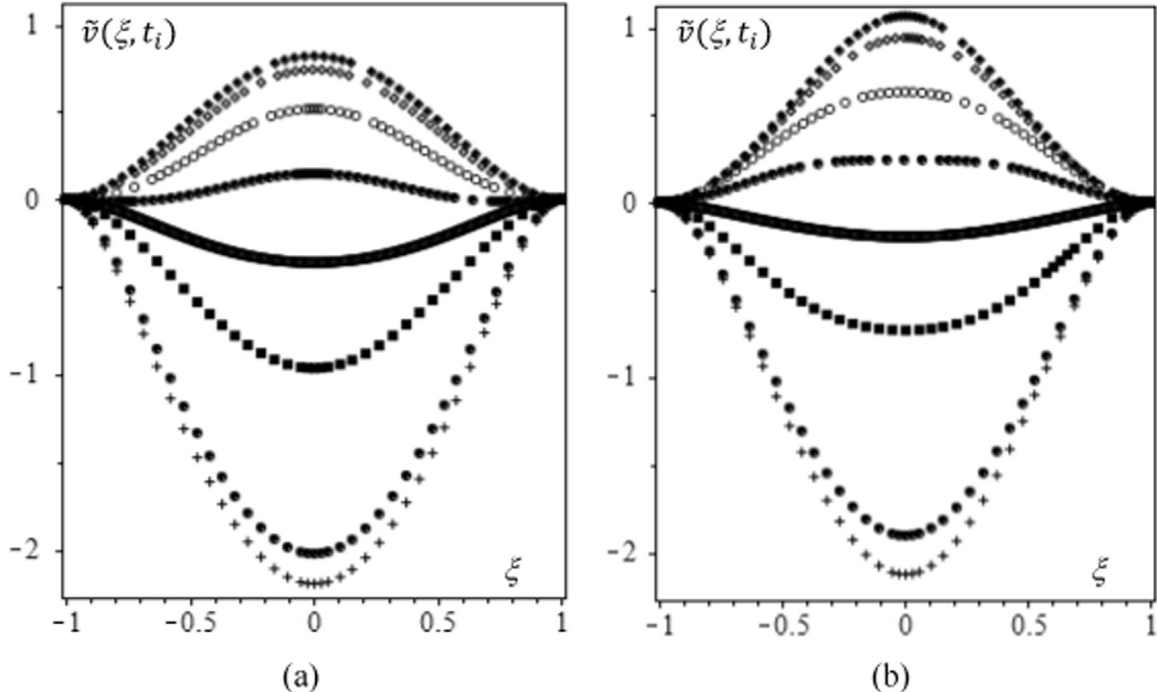


**Fig. 20.** Shapes of CNT at different instants along half a vibration period, when  $V=5$  V and (a)  $e_0a=0$ , in (b)  $e_0a=5.0$  nm. In both cases the amplitude of the first harmonic is approximately equal to  $1.5 \times 2R_{ext}$  ( $W_1(0)/(2R_{ext}) \approx 1.5$ ). The shapes at  $t=0$  s are represented by symbol ♦, the shapes at  $t=T/2$  s are represented by symbol +.

references [39,40], considering harmonic motions, and the same type of behaviour was found. When  $V=2.5$  V, a feeble softening appears, followed by hardening. As  $V$  increases further, so does the importance of softening and, eventually, the backbone curves become more complex, with more turning points. By increasing the DC voltage, one increases the static component of the CNT deflection, hence increasing the longitudinal tension. As the CNT oscillates with a relatively reduced oscillation amplitude about the deformed configuration, this initial tension decreases in the compression part of the cycles, hence softening appears. Further increasing the oscillation amplitude, the longitudinal tension starts to, in average and considering a complete vibration cycle, increase and, consequently, softening becomes hardening. Non-local effects alter the stiffness terms when the displacements are not small; furthermore, they affect the way in which the electrostatic force actuates the CNT. Due to the two former reasons, non-local effects influence the degrees of softening and hardening.

We will now analyse in more detail some of the responses, by investigating the magnitude of the constant term and the amplitudes of the first three harmonics. A positive or negative sign is attributed to these magnitudes, which are given by:

$$W_i(\xi) = \mathbf{f}_v(\xi)^T \mathbf{u}_i, \quad i = 0 - 3. \quad (39)$$

where  $\mathbf{u}_i$  are the coefficients of the harmonics, as in Eq. (31). For the sake of simplicity, we will designate the magnitude of the constant term as “constant term”, and the sign affected amplitudes of harmonics as “harmonics”.

First, we will consider case  $V=2$  V, with  $e_0a=0$  and  $e_0a=5.0$  nm. This case is interesting because there is still only hardening when  $V=2$  V, but the electric potential is large enough to originate backbone curves that are significantly different from the, more analysed in the literature, 0 V case (compare Fig. 10 and Fig. 8). Fig. 15 shows the constant term ( $W_0(0)/2$ ) and the first three harmonics at  $x=0$  ( $W_1(0)$ ,  $W_2(0)$  and  $W_3(0)$ ).

It was already obvious in Figs. 8–14 that the DC voltage introduces a vertical shift and an asymmetry in the transverse

displacement. Fig. 15 shows that this shift and this asymmetry occur because the signs of the constant term and second harmonic do not change, whilst the signs of odd harmonics do. Time plots to be shown afterwards will further illustrate this issue.

The constant term (Fig. 15a) decreases as the overall oscillation amplitude (shown in Fig. 10) increases. One possible reason behind this behaviour is the stiffening of the CNT as the vibration amplitude increases. Another factor that influences the constant term when oscillations occur, is that the electrostatic force varies asymmetrically along a vibration cycle, in the sense that it decreases/increases when the displacements are positive/negative; therefore the average value of the constant force varies with the amplitude of the oscillations. In the frequency range of Fig. 15, the first harmonic always increases with the natural frequency of vibration; the second harmonic amplitude first increases and then decreases, but the second harmonic is always small. The third harmonic is small in the local case ( $e_0a$  equal to 0) and for lower frequencies in the non-local case ( $e_0a$  equal to 5.0 nm). However, at larger frequencies, the amplitude of the third harmonic of the non-local CNT achieves large values. The non-local parameter affects the stiffness when the displacements are large; this change in stiffness promoted an interaction between the first and the third mode of vibration, leading to a growth of the third harmonic which does not occur in the local case.

Increasing the voltage to 5 V, still with  $e_0a=0$  or  $e_0a=5.0$  nm, the constant term and the harmonics shown in Fig. 16 are obtained. Understandably, the relative importance of the constant term and of the second harmonic is now much larger than in the 2 V case. This behaviour occurs because the increase in voltage led to a larger asymmetry of the system and, consequently, increased the importance of even non-linearities. Furthermore, initially there is softening, which is followed by hardening after a turning point; this behaviour is intimately connected with the longitudinal tension, as explained in a previous paragraph. The consideration of non-local effects ( $e_0a=5.0$  nm), not only leads to changes in the natural frequencies (again, due to an alteration of the stiffness), but also to a marked increase of the third harmonic, mainly

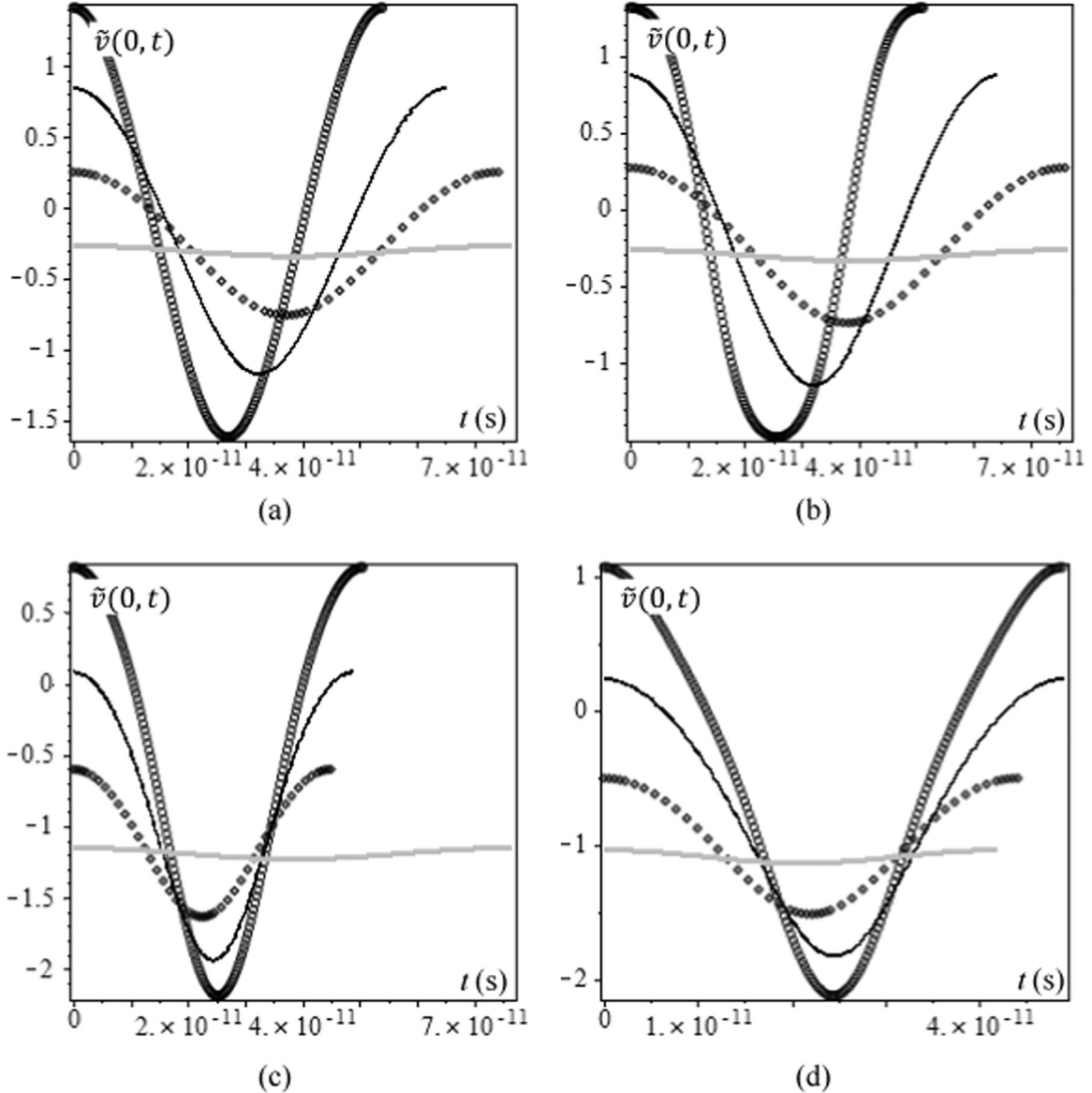


**Fig. 21.** Time histories of displacement of the middle point of CNT, with (a)  $V=2$  V,  $e_0a=0$ ; (b)  $V=2$  V,  $e_0a=5.0$  nm; (c)  $V=5$  V,  $e_0a=0$ ; (d)  $V=5$  V,  $e_0a=5.0$  nm. The solutions correspond to the following amplitudes of the first harmonic: —  $W_1(0)/(2R_{ext}) \approx 0$ ;  $\diamond$   $W_1(0)/(2R_{ext}) \approx 0.5$ ;  $\circ$   $W_1(0)/(2R_{ext}) \approx 1.0$ ;  $\square$   $W_1(0)/(2R_{ext}) \approx 1.5$ .

connected with the excitation of the third mode of vibration.

We saw in Fig. 15 and in Fig. 16 that for each natural frequency, there are two values for the odd harmonics, but only one for the constant term and for the second harmonic. The physical explanation for this behaviour is that the electrostatic force, which is responsible for the constant term and for the second harmonic, pulls the CNT towards the electrode. If the fact that the constant term exists due to the electrostatic force is obvious without resorting to equations, the relation between this force and the second harmonic becomes evident after we look at the equation of the electrostatic force (13): the even type non-linearities of this force cause the second harmonic. The other type of non-linearity of the system, which is geometrical, could, on its own, only introduce the second harmonic if symmetry breaking bifurcations occur [16], but these bifurcations are not investigated here. It results from these factors that the second harmonic and the constant term only have one sign, explaining the one solution per natural frequency, unlike the odd harmonics, for which there are two solutions per natural frequency (or more solutions, if a turning point is passed).

**3.2.2.2. Shapes of vibration.** In a study of modes of vibration, it is not enough to analyse the natural frequencies and the harmonic content of the oscillations, it is also important to see what happens with the shapes and this is the goal of this section. The shapes of the diverse harmonics are analysed and the evolutions of specific modes of vibration along time are also shown.

In Fig. 17, shapes assumed by the constant term and by each harmonic, when  $V=2$  V and  $e_0a$  is either equal to 0 or to 5.0 nm ( $\zeta=0.1$ ), are displayed. In order to show how they change, the shapes of the diverse harmonics are normalised so that the amplitude of any harmonic in the middle of the CNT is equal to one. Four solutions, distinguished by the amplitude of the first harmonic, are considered. Comparing the variation of the shapes with the vibration amplitude, one sees that, with or without non-local effects, the shape of the constant term is only slightly affected by the amplitude and the shape of the first harmonic barely changes (to see the minor variation, a zoom is required) with the vibration amplitude. When  $e_0a$  is equal to 0 nm, the shape of the second harmonic only experiences small changes; on the other hand, if the non-local parameter is 5.0 nm, then the shape of the second

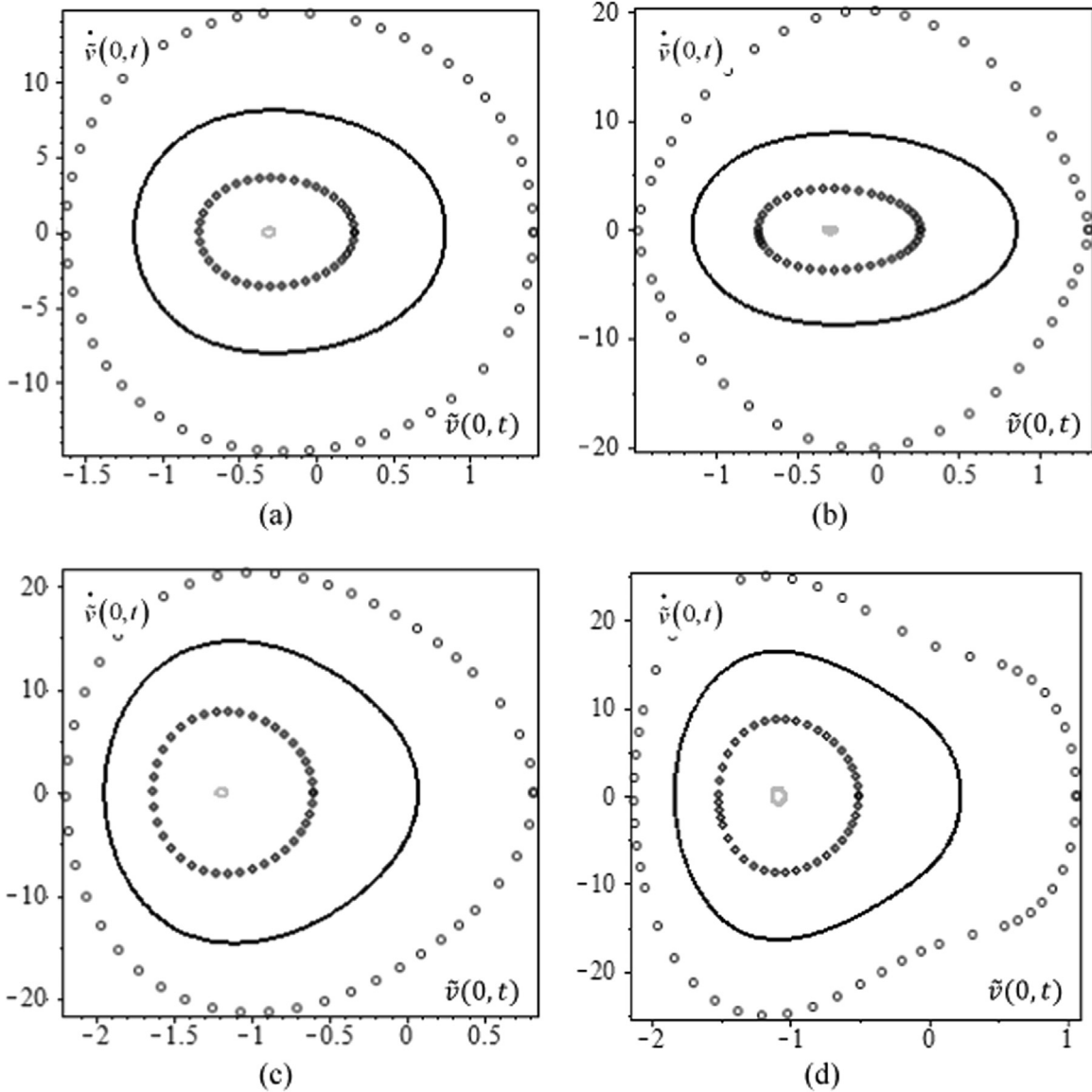


**Fig. 22.** Velocity versus displacement of the middle point of CNTs, with (a)  $V=2$  V,  $e_0a=0$ ; (b)  $V=2$  V,  $e_0a=5.0$  nm; (c)  $V=5$  V,  $e_0a=0$ ; (d)  $V=5$  V,  $e_0a=5.0$  nm. The solutions correspond to the following amplitudes of the first harmonic: —  $W_1(0)/(2R_{ext}) \geq 0$ ;  $\diamond W_1(0)/(2R_{ext}) \approx 0.5$ ;  $\square W_1(0)/(2R_{ext}) \approx 1.0$ ;  $\circ W_1(0)/(2R_{ext}) \approx 1.5$ .

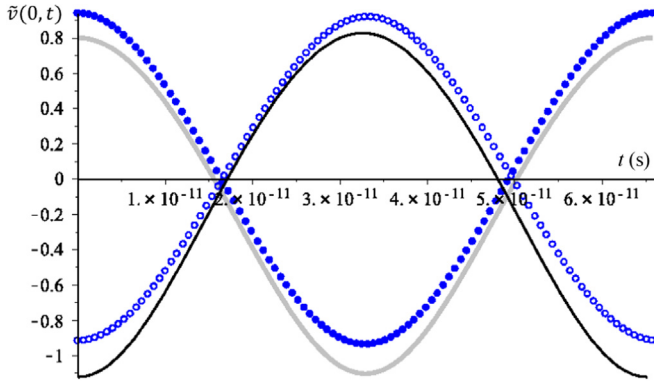


**Fig. 23.** Displacement of the middle point of the CNT as a function of time, when  $\tilde{\omega} \approx 28$  and  $e_0a=5$  nm. Solutions with  $V=0$  V: ● and ○. Solutions with  $V=2$  V: — and —.

harmonic significantly varies. Finally, the shape of the third harmonic is strongly affected by the oscillation amplitude and differs from the local to the non-local case. The shape of the third

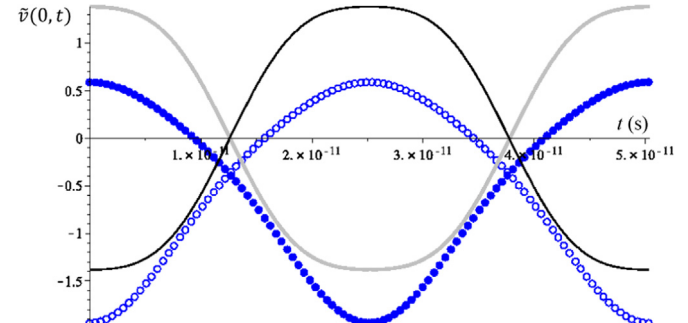


**Fig. 24.** Displacement of the middle point of the CNT as a function of time, when  $\tilde{\omega} \approx 36.6$  and  $e_0a=5$  nm. Solutions with  $V=0$  V: ● and ○. Solutions with  $V=2$  V: — and —.

harmonic is essentially defined by the first and second symmetric modes of vibration, with the relative importance of the second symmetric mode greater when  $W_1(0)/(2R_{ext}) \approx 1.5$ .

Now, in order to see the variation of the shape of the CNT along a vibration period, we consider the transverse deflection as given

by Eqs. (31) and (14). Examples of oscillations of the CNT along half a cycle are given in Fig. 18, considering the small scale effects, with  $e_0a=5.0$  nm, and despising them ( $e_0a=0$ ). In both oscillations, the amplitude of the first harmonic is approximately equal to  $1.5 \times 2R_{ext}$ . Fig. 18 illustrates how the modes of vibration evolve in time. Furthermore, Fig. 18 illustrates that the modes of vibration that correspond to the same amplitude of the first harmonic are different with and without non-local effects. Another difference between these two modes occurs in their natural frequencies of vibration: the amplitude of the first harmonic is approximately equal to  $1.5 \times 2R_{ext}$  at  $1.16 \times 10^{11}$  rad/s in the local case and at  $1.22 \times 10^{11}$  rad/s in the non-local case. Visibly, the shapes that the CNT assumes along a vibration period are not equal to the first linear mode shape.

In Fig. 19, the shapes assumed by the constant term and each harmonic are shown, again in non-local case with  $e_0a=5.0$  nm and in the local case, but now with  $V=5$  V. The variation of the shapes with the oscillation amplitude are much more important in the second and third harmonic, than in the first harmonic or in the constant term (in the last two cases, variations are small and best seen if the pictures are amplified).

Plotting snapshots of the CNT actuated by a DC voltage equal to 5 V, at different instants along half a vibration period, complements our understanding of the mode of vibration. Fig. 20 shows such shapes for a specific amplitude of the first harmonic ( $1.5 \times 2R_{ext}$ ), again considering the small scale effects, with  $e_0a=5.0$  nm, and despising them ( $e_0a=0$ ). As occurred in the 2 V case, the non-local effects alter the non-linear mode of vibration, with the influence of the second symmetric mode more visible in the non-local than in the local case. The inward displacement magnitude achieves – with and without non-local effects – larger values now than when  $V=2$  V, at the detriment of the upward motion. Curiously, with the non-local model, the CNT achieves larger positive deflections and not so large, in absolute value, negative values. These differences between the local and non-local CNT are due to the higher harmonics and to the constant term, as the backbone curves demonstrate. The frequency at which the first harmonic achieves amplitude  $1.5 \times 2R_{ext}$  also differs: it is  $1.29 \times 10^{11}$  rad/s in the local case, and  $1.24 \times 10^{11}$  rad/s in the non-local case.

**3.2.2.3. Time and phase plots.** To further illustrate the influence of DC voltage and non-local effects on the modes of vibration, plots of time histories and projections of trajectories on a phase plane (designated here as phase plots) are shown in Fig. 21 and in Fig. 22, respectively. The non-dimensional velocity is given by

$$\dot{\tilde{v}}(\xi, t) = \frac{\dot{v}(\xi, t)T}{2R_{ext}}, \quad (40)$$

where  $T$  represents the period of vibration. The solutions are chosen according to the corresponding amplitudes of the first harmonic. It is evident that the vibration period decreases as the vibration amplitude increases, when  $V=2$  V. It is also visible that the non-local effects alter the time response, when  $V=2$  V. When  $V=5$  V, whilst the vibration period first decreases and then increases as the vibration amplitude increases in the local case, in the non-local case the period of vibration always increases with the vibration amplitude (in the range portrayed). The asymmetry of the oscillations is evident in all time and phase plots, but it is more pronounced when  $V=5$  V and non-local effects are taken into account.

Finally, in order to complete our explanation of the asymmetries found in Figs. 9–14, we refer to Figs. 23 and 24. These figures show the variation with time of the transverse component of the displacement of the middle point of the CNT, for initial deflections on one or on the other side of the statically deformed CNT, the

same is to say, for cases where the first harmonics have the same amplitude but different signs/phases. When voltage is zero, so are the constant term and the second harmonic; therefore, the time responses are symmetric about the horizontal axis. On the other hand, when the voltage is not zero, the time responses occur about a horizontal axis that is shifted in the vertical direction, due to the constant term; furthermore, the oscillations stop being symmetric about the shifted horizontal axis, because of the second harmonic. The latter is in particular important in Fig. 24 when  $V$  is 5 V. We note that in this figure, none of the time histories is sinusoidal, but the first and third harmonics are the most important when  $V$  is 0 V, whilst the first and the second harmonics are the most important when  $V$  is 5 V. In summary, the absolute values of the transverse displacement when  $t=0$  s are substantially different if the CNT is initially deflected in one or in the other direction because of the asymmetry of the system under analysis when a DC voltage is applied.

#### 4. Conclusions

In this manuscript, a Bernoulli–Euler  $p$ -version FEM type formulation that applies to carbon nanotubes under the action of electrostatic forces was presented. Results computed with the numerical model implemented were successfully compared with a number of published results. Afterwards, the modes of vibration in the non-linear regime were investigated. Backbone curves defined by the vibration displacement at the beginning of the cycle, versus the natural frequency of vibration, were presented and analysed first. Then, in selected cases, the analyses were complemented with examinations of the amplitudes of each harmonic, of the shapes assumed by the harmonics and by the CNT along a vibration period, and with time and phase plane plots.

Data was computed for different values of the applied voltage. Larger voltages lead to larger natural frequencies at very low (infinitesimally small) amplitudes of vibration. This low vibration amplitude frequency is not a “linear frequency”, because the oscillations occur about a deformed configuration due to the electrostatically induced deflection of the CNT. Hence, the system cannot be considered to be in the linear regime. The increase with voltage of the natural frequency of vibration at low vibration amplitudes is due to the tension that develops under the static component of deflection (let’s designate it as “initial tension”). When the voltage is low, the frequency of vibration increases with the vibration amplitude, because the longitudinal tensions increase with the oscillation. But at larger voltages, hence larger initial tensions, softening initially appears because the average tension decreases along a cycle of vibration about the deformed configuration; this decrease occurs because the initial tension alleviates in part of the cycle (as if compression occurred). At sufficiently large vibration amplitudes, softening is replaced by hardening, after a turning point, because, considering its average along a cycle of vibration, the longitudinal tension increases with the larger vibration amplitudes.

Non-local effects, the geometrical non-linearity and the non-linear electrostatic force interact in a complex way. It was found that all influence the degree of hardening or softening. The consideration of non-local effect when the voltage is low, leads to a decrease in the frequency at low amplitudes of vibration, due to an augmentation of inertia. But at larger voltages the consideration of non-local effects results in an increase of the same frequency, in spite of the increased inertia. This is due to the stiffening caused by non-local effects when the geometrical non-linearity is considered (recall that with larger voltages the geometrical non-linear terms become important even when the vibration amplitude is low, because of the static component of deflections).

Non-local effects also influence the shape of vibration of the CNTs along a free vibration cycle. Since non-local effects alter mass and stiffness, it is not a surprise that they alter the mode shape of vibration. It was verified that the shapes the CNTs assume during a vibration period are not equal to the first linear mode shape. The major influence that the non-local effect has on the shape assumed by the CNT along a vibration cycle, is connected with the internal resonance phenomenon. Non-locality, by changing the stiffness and inertia, alters the conditions for internal resonances. Therefore, we found examples where non-local effects called into the motion a higher order mode, under an internal resonance that does not occur – or does not occur for the same natural frequency – in the local CNT.

It was shown that, when voltage is not zero, the problem becomes non-symmetric. To start with, the equilibrium configuration of the CNT is a curved one. In this case, oscillations that correspond to initial displacements taking place in opposite directions differ in the relative phase of the diverse harmonics, in this way affecting the time response and the magnitude of the displacement in the beginning of a vibration cycle.

The author believes that the knowledge gained from the present study on the modes of vibration of electrostatically actuated CNT is important to understand the dynamic behaviour of this type of system. The variations of the natural frequency – with the voltage or with the vibration amplitude – which were described here, indicate what is likely to occur with resonance frequencies in forced vibration. The variations of the mode shapes can also be important in applications, since they lead to different displacements; the modal interactions found in this paper can eventually be applied in the design of sensors or energy harvesters.

## Acknowledgements

The initial part of this work was performed at Arts et Métiers Paris Tech, Lille campus, in a sabbatical stay. The author acknowledges the financial support of the Portuguese Science and Technology foundation (FCT), under sabbatical Grant SFRH/BSAB/1442/2014, and Prof. Olivier Thomas for kindly hosting his stay in Lille.

## References

- [1] K. Eom, H.S. Park, D.S. Yoon, T. Kwon, Nanomechanical resonators and their applications in biological/chemical detection: nanomechanics principles, *Phys. Rep.* 503 (2011) 115–163.
- [2] K.L. Ekinci, Electromechanical transducers at the nanoscale: actuation and sensing of motion in nanoelectromechanical systems (NEMS), *Small* 1 (2005) 86–797.
- [3] H.B. Peng, C.W. Chang, S. Aloni, T.D. Yuzvinsky, A. Zett, Ultrahigh frequency nanotube resonators, *Phys. Rev. Lett.* 97 (2006) 087203–087204.
- [4] Y.T. Yang, C. Callegari, X.L. Feng, K.L. Ekinci, M.L. Roukes, Zeptogram-scale nanomechanical mass sensing, *Nano Lett.* 6 (2006) 583–586.
- [5] A.K. Naik, M.S. Hanay, W.K. Hiebert, X.L. Feng, M.L. Roukes, Towards single-molecule nanomechanical mass spectrometry, *Nat. Immunol.* 4 (2009) 445–450.
- [6] B. Arash, J.W. Jiang, T. Rabczuk, A review on nanomechanical resonators and their applications in sensors and molecular transportation, *Appl. Phys. Rev.* 2 (2015).
- [7] R.F. Gibson, E.O. Ayorinde, Y.-F. Wen, Vibrations of carbon nanotubes and their composites: a review, *Composites Sci. Technol.* 67 (2007) 1–28.
- [8] H.M. Ouakad, M.I. Younis, Nonlinear dynamics of electrically actuated carbon nanotube resonators, *J. Comput. Nonlinear Dyn.* 5 (2010).
- [9] R.B. Karabalin, S.C. Masmanidis, M.L. Roukes, Efficient parametric amplification in high and very high frequency piezoelectric nanoelectromechanical systems, *Appl. Phys. Lett.* 97 (2010) 183101.
- [10] A. Lazarus, O. Thomas, J.F. Deü, Finite element reduced order models for nonlinear vibrations of piezoelectric layered beams with applications to NEMS, *Finite Elem. Anal. Des.* 49 (2012) 35–51.
- [11] V.N. Nguyen, S. Baguet, C.H. Lamarque, R. Dufour, Bifurcation-based micro-/nanoelectromechanical mass detection, *Nonlinear Dyn.* 79 (2015) 647–662.
- [12] M.H. Matheny, L.G. Villanueva, R.B. Karabalin, J.E. Sader, M.L. Roukes, Non-linear mode-coupling in nanomechanical systems, *Nano Lett.* 13 (2013) 1622–1626.
- [13] O. Thomas, F. Mathieu, W. Mansfield, C. Huang, S. Trolier-McKinstry, L. Nicu, Efficient parametric amplification in micro-resonators with integrated piezoelectric actuation and sensing capabilities, *Appl. Phys. Lett.* 102 (2013).
- [14] R. Lewandowski, Nonlinear free-vibrations of beams by the finite-element and continuation methods, *J. Sound Vib.* 170 (1994) 577–593.
- [15] P. Ribeiro, M. Petry, Non-linear vibration of beams with internal resonance by the hierarchical finite-element method, *J. Sound Vib.* 224 (1999) 591–624.
- [16] S. Stoykov, P. Ribeiro, Nonlinear free vibrations of beams in space due to internal resonance, *J. Sound Vib.* 330 (2011) 4574–4595.
- [17] C. Touzé, O. Thomas, A. Huberdeau, Asymptotic non-linear normal modes for large-amplitude vibrations of continuous structures, *Comput. Struct.* 82 (2004) 2671–2682.
- [18] W.-M. Zhang, H. Yan, Z.-K. Peng, G. Meng, Electrostatic pull-in instability in MEMS/NEMS: a review, *Sens. Actuators A: Phys.* 214 (2014) 187–218.
- [19] R.M.C. Mestrom, R.H.B. Fey, K.L. Phan, H. Nijmeijer, Simulations and experiments of hardening and softening resonances in a clamped-clamped beam MEMS resonator, *Sens. Actuators A - Phys.* 162 (2010) 225–234.
- [20] M.H. Ghayesh, M. Amabili, H. Farokhi, Nonlinear forced vibrations of a microbeam based on the strain gradient elasticity theory, *Int. J. Eng. Sci.* 63 (2013) 52–60.
- [21] H.M. Ouakad, M.I. Younis, Natural frequencies and mode shapes of initially curved carbon nanotube resonators under electric excitation, *J. Sound Vib.* 330 (2011) 3182–3195.
- [22] T.T. Xu, M.I. Younis, Nonlinear dynamics of carbon nanotubes under large electrostatic force, *J. Comput. Nonlinear Dyn.* 11 (2016).
- [23] M.I. Younis, A.H. Nayfeh, A study of the nonlinear response of a resonant microbeam to an electric actuation, *Nonlinear Dyn.* 31 (2003) 91–117.
- [24] D.I. Caruntu, L. Luo, Frequency response of primary resonance of electrostatically actuated CNT cantilevers, *Nonlinear Dyn.* 78 (2014) 1827–1837.
- [25] M. Dequesnes, S.V. Rotkin, N.R. Aluru, Calculation of pull-in voltages for carbon-nanotube-based nanoelectromechanical switches, *Nanotechnology* 13 (2002) 120–131.
- [26] C.H. Ke, H.D. Espinosa, N. Pugno, Numerical analysis of nanotube based NEMS devices – Part II: role of finite kinematics, stretching and charge concentrations, *J. Appl. Mech. Trans. ASME* 72 (2005) 726–731.
- [27] M.M.S. Fakhraabadi, A. Rastgo, M.T. Ahmadian, Size-dependent instability of carbon nanotubes under electrostatic actuation using nonlocal elasticity, *Int. J. Mech. Sci.* 80 (2014) 144–152.
- [28] M. Rasekh, S.E. Khadem, Pull-in analysis of an electrostatically actuated nanocantilever beam with nonlinearity in curvature and inertia, *Int. J. Mech. Sci.* 53 (2011) 108–115.
- [29] M.M.S. Fakhraabadi, A. Rastgo, M.T. Ahmadian, Non-linear behaviors of carbon nanotubes under electrostatic actuation based on strain gradient theory, *Int. J. Non-Linear Mech.* 67 (2014) 236–244.
- [30] P. Kasirajan, R. Amirtham, J.N. Reddy, Surface and non-local effects for nonlinear analysis of Timoshenko beams, *Int. J. Non-Linear Mech.* 76 (2015) 100–111.
- [31] A.C. Eringen, Linear theory of nonlocal elasticity and dispersion of plane waves, *Int. J. Eng. Sci.* 10 (1972) 425–435.
- [32] A. Eringen, On differential equations of nonlocal elasticity and solutions of screw dislocation and surface waves, *J. Appl. Phys.* 54 (1983) 8.
- [33] Y. Chen, J.D. Lee, A. Eskandarian, Atomistic viewpoint of the applicability of microcontinuum theories, *Int. J. Solids Struct.* 41 (2004) 2085–2097.
- [34] R. Ansari, S. Sahmani, Small scale effect on vibrational response of single-walled carbon nanotubes with different boundary conditions based on non-local beam models, *Commun. Nonlinear Sci. Numer. Simul.* 17 (2012) 1965–1979.
- [35] N.M. Ghoniem, E.P. Busso, N. Kioussis, H. Huang, Multiscale modelling of nanomechanics and micromechanics: an overview, *Philos. Mag.* 83 (2003) 3475–3528.
- [36] B. Arash, Q. Wang, A review on the application of nonlocal elastic models in modeling of carbon nanotubes and graphenes, *Comput. Mater. Sci.* 51 (2012) 303–313.
- [37] L.F. Wang, H.Y. Hu, Flexural wave propagation in single-walled carbon nanotubes, *Phys. Rev. B* 71 (2005).
- [38] Y.-G. Hu, K.M. Liew, Q. Wang, Nonlocal elastic beam models for flexural wave propagation in double-walled carbon nanotubes, *J. Appl. Phys.* 106 (2009) 044301.
- [39] J. Yang, L.L. Ke, S. Kitipornchai, Nonlinear free vibration of single-walled carbon nanotubes using nonlocal Timoshenko beam theory, *Physica E* 42 (2010) 1727–1735.
- [40] M. Şimşek, Large amplitude free vibration of nanobeams with various boundary conditions based on the nonlocal elasticity theory, *Composites: Part B* 56 (2014) 621–628.
- [41] J.N. Reddy, Nonlocal theories for bending, buckling and vibration of beams, *Int. J. Eng. Sci.* 45 (2007) 288–307.
- [42] J.N. Reddy, Nonlocal nonlinear formulations for bending of classical and shear deformation of beams and plates, *Int. J. Eng. Sci.* 48 (2010) 1507–1518.
- [43] R. Lewandowski, Solutions with bifurcation points for free-vibration of beams – an analytical approach, *J. Sound Vib.* 177 (1994) 239–249.
- [44] C.E. Ke, D. Horacio, Numerical analysis of nanotube-based NEMS devices—Part I: electrostatic charge distribution on multiwalled nanotubes, *J. Appl. Mech.* 72 (2005) 721–725.
- [45] P. Ribeiro, O. Thomas, Modes of Vibration of Non-local Beams Vibrating with

- Large Amplitude Displacements, Submitted for publication, 2015.
- [46] W. Han, M. Petyt, K.M. Hsiao, An investigation into geometrically non-linear analysis of rectangular laminated plates using the hierarchical finite element method, *Finite Elem. Anal. Des.* 18 (1994) 273–288.
- [47] P. Ribeiro, Hierarchical finite element analyses of geometrically non-linear vibration of beams and plane frames, *J. Sound Vib.* 246 (2001) 225–244.
- [48] N.S. Bardell, Free-vibration analysis of a flat-plate using the hierarchical finite-element method, *J. Sound Vib.* 151 (1991) 263–289.
- [49] P. Ribeiro, Non-linear free periodic vibrations of open cylindrical shallow shells, *J. Sound Vib.* 313 (2008) 224–245.
- [50] P. Ribeiro, Non-linear modes of vibration of thin cylindrical shells in composite laminates with curvilinear fibres, *Compos. Struct.* 122 (2015) 184–197.
- [51] R. Lewandowski, Computational formulation for periodic vibration of geometrically nonlinear structures 0.2. Numerical strategy and examples, *Int. J. Solids Struct.* 34 (1997) 1949–1964.
- [52] P. Ribeiro, M. Petyt, Non-linear free vibration of isotropic plates with internal resonance, *Int. J. Non-Linear Mech.* 35 (2000) 263–278.
- [53] M. Dequesnes, Z. Tang, N.R. Aluru, Static and dynamics analysis of carbon nanotube-based switches, *J. Eng. Mater. Technol.* 126 (2004) 230–237.
- [54] M.H. Ghayesh, Nonlinear size-dependent behaviour of single-walled carbon nanotubes, *Appl. Phys. A* 117 (2014) 1393–1399.
- [55] M.M.J. Treacy, T.W. Ebbesen, J.M. Gibson, Exceptionally high Young's modulus observed for individual carbon nanotubes, *Nature* 381 (1996).
- [56] Z.L. Wang, R.P. Gao, P. Poncharal, W.A. de Heer, Z.R. Dai, Z.W. Pan, Mechanical and electrostatic properties of carbon nanotubes and nanowires, *Mater. Sci. Eng. C – Biol. Sci.* 16 (2001) 3–10.
- [57] C.Y. Li, T.W. Chou, A structural mechanics approach for the analysis of carbon nanotubes, *Int. J. Solids Struct.* 40 (2003) 2487–2499.
- [58] J.R. Xiao, B.A. Gama, J.W. Gillespie, An analytical molecular structural mechanics model for the mechanical properties of carbon nanotubes, *Int. J. Solids Struct.* 42 (2005) 3075–3092.
- [59] J. Yoon, C.Q. Ru, A. Mioduchowski, Vibration of an embedded multiwall carbon nanotube, *Compos. Sci. Technol.* 63 (2003) 1533–1542.
- [60] M.F. Yu, Fundamental mechanical properties of carbon nanotubes: current understanding and the related experimental studies, *J. Eng. Mater. Technol. ASME* 126 (2004) 271–278.
- [61] Q. Wang, Wave propagation in carbon nanotubes via nonlocal continuum mechanics, *J. Appl. Phys.* 98 (2005).
- [62] A. Krishnan, E. DuJardin, T.W. Ebbesen, P.N. Yianilos, M.M.J. Treacy, Young's modulus of single-walled nanotubes, *Phys. Rev. B* 58 (1998) 14013–14019.
- [63] P.J. Mohr, B.N. Taylor, D.B. Newell, CODATA recommended values of the fundamental physical constants: 2006, *Rev. Mod. Phys.* (2008) 633–730.
- [64] M.A. Eltaher, A.E. Alshorbagy, F.F. Mahmoud, Vibration analysis of Euler-Bernoulli nanobeams by using finite element method, *Appl. Math. Model.* 37 (2013) 4787–4797.
- [65] M. Simsek, Large amplitude free vibration of nanobeams with various boundary conditions based on the nonlocal elasticity theory, *Composites: Part B* 56 (2014) 8.
- [66] H.-T. Thai, A nonlocal beam theory for bending, buckling, and vibration of nanobeams, *Int. J. Eng. Sci.* 52 (2012) 56–64.